Inorg. Chem. **2008**, *47*, 11018−11031

Construction of Copper Halide-Triiron Selenide Carbonyl Complexes: Synthetic, Electrochemical, and Theoretical Studies

Minghuey Shieh,* Chia-Yeh Miu, Chang-Ju Lee, Wei-Cheng Chen, Yen-Yi Chu, and Hui-Lung Chen

Department of Chemistry, National Taiwan Normal University, Taipei 116, Taiwan, Republic of China

Received July 8, 2008

A new family of CuX-, Cu_2X_2-, and Cu_4X_2-incorporated mono- or di-$SeFe_3$-based carbonyl clusters were constructed and structurally characterized. When the selenium-capped triiron carbonyl cluster $[Et_4N]_2[SeFe_3(CO)_9]$ was treated with 1−3 equiv of CuX in tetrahydrofuran (THF) at low or room temperatures, CuX-incorporated $SeFe_3$ complexes $[Et_4N]_2[SeFe_3(CO)_9CuX]$ (X = Cl, $[Et_4N]_2$[**1a**]; Br, $[Et_4N]_2$[**1b**]; I, $[Et_4N]_2$[**1c**]), Cu_2X_2-incorporated $SeFe_3$ clusters $[Et_4N]_2[SeFe_3(CO)_9Cu_2X_2]$ (X = Cl, $[Et_4N]_2$[**2a**]; Br, $[Et_4N]_2$[**2b**]), and Cu_4X_2-linked di-$SeFe_3$ clusters $[Et_4N]_2[\{SeFe_3(CO)_9\}_2Cu_4X_2]$ (X = Cl, $[Et_4N]_2$[**3a**]; Br, $[PPh_4]_2$[**3b**]) were obtained, respectively, in good yields. $SeFe_3CuX$ complexes **1a** and **1b** were found to undergo cluster expansion to form $SeFe_3Cu_2X_2$ complexes **2a** and **2b**, respectively, upon the addition of 1 equiv of CuX (X = Cl, Br). Furthermore, complexes **2a** and **2b** can expand further to form Cu_4X_2-linked di-$SeFe_3$ clusters **3a** and **3b**, upon treatment with 1 equiv of CuX (X = Cl, Br). $[Et_4N]_4[\{SeFe_3(CO)_9(CuCl)_2\}_2]$ ($[Et_4N]_4$[**4a**]) was produced when the reaction of $[Et_4N]_2[SeFe_3(CO)_9]$ with 2 equiv of CuCl was conducted in THF at 40 °C. The Cu_2Cl_2-linked di-$SeFe_3CuCl$ cluster **4a** is a dimerization product derived from complex **2a**. Further, it is found that complex **4a** can convert to the Cu_4Cl_2-linked di-$SeFe_3$ cluster **3a** upon treatment with CuCl. The nature, formation, stepwise cluster expansion, and electrochemical properties of these CuX-, Cu_2X_2-, and Cu_4X_2-incorporated mono- or di-$SeFe_3$-based clusters are elucidated in detail by molecular calculations at the B3LYP level of the density functional theory in terms of the effects of selenium, iron, copper halides, and the size of the metal skeleton.

Introduction

The construction of extended frameworks based on transition metal and organometallic complexes has been an attractive area of contemporary chemistry.[1,2] Soluble transition metal carbonyl sulfide complexes have been extensively studied mainly because of their biological and catalytic activities. However, reports on the chemistry of their heavier selenium analogue have been relatively rare.[3] Apart from the lack of synthetic routes, the effect of selenium on the formation of the resultant transition metal complexes with various sizes is seldom systematically investigated.[3,4] With respect to the size of metal complexes, studies of the controlled growth and aggregation of homo- or heterometal clusters, which is an important issue in the current study of nanotechnology, have been rare. Our continuing interest in main group element-incorporated iron carbonyl clusters[5,6] prompted exploration of the possibility of employing such

* To whom correspondence should be addressed. E-mail: mshieh@ntnu.edu.tw.

(1) (a) *Comprehensive Supramolecular Chemistry*; Lehn, J.-M., Atwood, J. L., Davies, J. E. D., MacNicol, D. D., Vögtle, F., Eds.; Pergamon: Oxford, 1996. (b) Leininger, S.; Olenyuk, B.; Stang, P. J. *Chem. Rev.* **2000**, *100*, 853. (c) Gianneschi, N. C.; Masar, M. S., III; Mirkin, C. A. *Acc. Chem. Res.* **2005**, *38*, 825. (d) Robin, A. Y.; Fromm, K. M. *Coord. Chem. Rev.* **2006**, *250*, 2127. (e) Selby, H. D.; Roland, B. K.; Zheng, Z. *Acc. Chem. Res.* **2003**, *36*, 933. (f) Lang, J.-P.; Ji, S.-J.; Xu, Q.-F.; Shen, Q.; Tatsumi, K. *Coord. Chem. Rev.* **2003**, *241*, 47. (g) Gabriel, J.-C. P.; Boubekeur, K.; Uriel, S.; Batail, P. *Chem. Rev.* **2001**, *101*, 2037. (h) Bai, J.; Virovets, A. V.; Scheer, M. *Science* **2003**, *300*, 781.

(2) (a) Femoni, C.; Kaswalder, F.; Iapalucci, M. C.; Longoni, G.; Zacchini, S. *Chem. Commun.* **2006**, 2135. (b) Bai, J.; Leiner, E.; Scheer, M. *Angew. Chem., Int. Ed.* **2002**, *41*, 783. (c) Bai, J.; Virovets, A. V.; Scheer, M. *Angew. Chem., Int. Ed.* **2002**, *41*, 1737. (d) Nakajima, T.; Ishiguro, A.; Wakatsuki, Y. *Angew. Chem., Int. Ed.* **2001**, *40*, 1066. (e) Shieh, M.; Hsu, M.-H.; Sheu, W.-S.; Jang, L.-F.; Lin, S.-F.; Chu, Y.-Y.; Miu, C.-Y.; Lai, Y.-W.; Liu, H.-L.; Her, J. L. *Chem.—Eur. J.* **2007**, *13*, 6605.

(3) (a) *The Chemistry of Metal Cluster Complexes*; Shriver, D. F., Kaesz, H. D., Adams, R. D., Eds.; Wiley-VCH Publishers: New York, 1990. (b) *Metal Clusters in Chemistry*; Braunstein, P., Oro, L. A., Raithby, P. R., Eds.; Wiley-VCH Publishers: Weinheim, 1999; Vols. *1*− *3*. (c) Roof, L. C.; Kolis, J. W. *Chem. Rev.* **1993**, *93*, 1037. (d) Mathur, P. *Adv. Organomet. Chem.* **1997**, *41*, 243. (e) Sekar, P.; Ibers, J. A. *Inorg. Chem.* **2002**, *41*, 450, and references therein. (f) Shieh, M. *J. Cluster Sci.* **1999**, *10*, 3.

10.1021/ic8012552 CCC: $40.75
Published on Web 10/30/2008

complexes as building blocks to probe the complicated coupling effect of main group elements and transition metals on their aggregation and expansion reactions.

Copper halides have been established as a preparative tool with respect to the synthesis of adduct compounds with new polymeric and oligomeric main group molecules.[7] Besides, it is thought that copper halides are effective linkers for the connection of such iron-containing carbonyl clusters because of the ease of their redox behavior[8] and their softness which can facilitate their affinity toward late transition metals. In view of their potential use as solid-state materials, Cu(I) ions exhibit high conductivity, which often is reflected in their compounds.[4b,9] For example, the ternary $CuFeS_2$ has long been known to be a semiconductor material[9a] while only limited information about $CuFeSe_2$ has been revealed.[9b] With these perspectives, we treated the selenium-capped triiron carbonyl complex[6b,10] $[SeFe_3(CO)_9]^{2-}$ with a series of CuX (X = Cl, Br, I) to explore its potential as a good building unit because of the softness and the comparative size of Se and Fe and also to probe the coupled effect of Se and Fe atoms on their resultant clusters in terms of different copper halides.

In this work, a new series of copper halide-incorporated mono- or di-$SeFe_3$-based carbonyl complexes has been achieved and systematically compared for the first time in terms of the effect of halides and the size of the metal skeleton. The synthesis, stepwise cluster expansion, and electrochemistry of these Se—Fe—Cu clusters were further examined in detail by molecular calculations at the B3LYP level of the density functional theory (DFT).

Results and Discussion

Reaction of $[Et_4N]_2[SeFe_3(CO)_9]$ with 1 equiv of CuX (X = Cl, Br, I). When the selenium-capped triiron carbonyl cluster $[Et_4N]_2[SeFe_3(CO)_9]$[6b,10c] was treated with CuX (X = Cl, Br, I) in tetrahydrofuran (THF) solutions in an ice−water bath, CuX-incorporated $SeFe_3$-based carbonyl complexes $[Et_4N]_2[SeFe_3(CO)_9CuX]$ (X = Cl, $[Et_4N]_2$[**1a**]; Br, $[Et_4N]_2$[**1b**]; I, $[Et_4N]_2$[**1c**]) were produced (Scheme 1). These reactions proceeded smoothly within approximately 10 min with formation of clusters **1a**−**1c** in good yields.

Complexes **1a**, **1b**, and **1c** were fully characterized by spectroscopic methods and single-crystal X-ray analysis. The X-ray analysis shows that **1a**, **1b**, and **1c** are isomorphous and each exhibits an $SeFe_3$ core with each Fe atom terminally coordinated by three carbonyls, in which one of the Fe—Fe bonds is bridged by one Cu that is bound to the X atom (X = Cl, **1a**; Br, **1b**; I, **1c**) (Figures 1−3). The IR of **1a**, **1b**, and **1c** show the absorptions characteristic of terminal carbonyls, with the pattern similar to that of the parent cluster $[SeFe_3(CO)_9]^{2-}$ but absorption frequencies shifted to higher energies (See Table 1) because of the electron-withdrawing effect of CuX (X = Cl, Br, I).

Reaction of $[Et_4N]_2[SeFe_3(CO)_9]$ with 2 equiv of CuX (X = Cl, Br, I). In the case of CuX (X = Cl, Br), the reaction of $[Et_4N]_2[SeFe_3(CO)_9]$ with 2 equiv of CuX in THF solutions at −30 °C produced Cu_2X_2-incorporated clusters $[Et_4N]_2[SeFe_3(CO)_9Cu_2X_2]$ (X = Cl, $[Et_4N]_2$[**2a**]; Br, $[Et_4N]_2$[**2b**]), respectively (Scheme 1). However, a similar reaction with 2 equiv of CuI in THF failed to give the analogous Cu_2I_2-incorporated cluster probably because of its lower stability.

$[Et_4N]_2$[**2a**] and $[Et_4N]_2$[**2b**] were fully characterized by X-ray analysis and spectroscopic methods. Clusters **2a** and **2b** each were shown by the X-ray analysis to display a $SeFe_3$ core with one Fe—Fe edge bridged by a Cu atom in which the Fe_3Cu butterfly is capped by another Cu atom with the two Cu atoms further bound to the X atoms (X = Cl, **2a**; Br, **2b**) (Figures 4,5). Alternatively, cluster **2a** or **2b** can also be viewed to contain a Se-capped Fe_3Cu_2 trigonal bipyramidal core with the μ_4-CuX fragment in the equatorial position and the μ_3-CuX fragment in the axial position. It is noted that $[Et_4N]_2$[**2a**] and $[Et_4N]_2$[**2b**] can be isolated at −30 to ∼0 °C and are stable in solids. Their existence is further substantiated by their powder X-ray diffraction (XRD) patterns which are in good agreement with those calculated from single-crystal XRD.

Reaction of $[Et_4N]_2[SeFe_3(CO)_9]$ with 3 equiv of CuX (X = Cl, Br). Further investigation into the use of $[Et_4N]_2[SeFe_3(CO)_9]$ as a building block, with increased amounts of CuX, to form other $SeFe_3$-based expanded framework was carried out. The results showed that $[Et_4N]_2[SeFe_3(CO)_9]$ could react readily with 3 equiv of CuX in THF solutions at room temperature to form Cu_4X_2-linked di-$SeFe_3$ clusters $[Et_4N]_2[\{SeFe_3(CO)_9\}_2Cu_4X_2]$ (X = Cl,

(4) (a) Dehnen, S.; Eichhöfer, A.; Fenske, D. *Eur. J. Inorg. Chem.* **2002**, 279. (b) Eichhöfer, A.; Fenske, D.; Olkowska-Oetzel, J. *Eur. J. Inorg. Chem.* **2007**, 74. (c) Nitschke, C.; Fenske, D.; Corrigan, J. F. *Inorg. Chem.* **2006**, *45*, 9394, and references therein. (d) Lackmann, J.; Hauptmann, R.; Weißgräber, S.; Henkel, G. *Chem. Commun.* **1999**, 1995. (e) Wallbank, A. I.; Borecki, A.; Taylor, N. J.; Corrigan, J. F. *Organometallics* **2005**, *24*, 788.

(5) (a) Shieh, M.; Liou, Y.; Hsu, M.-H.; Chen, R.-T.; Yeh, S.-J.; Peng, S.-M.; Lee, G.-H. *Angew. Chem., Int. Ed.* **2002**, *41*, 2384. (b) Shieh, M.; Liou, Y.; Peng, S.-M.; Lee, G.-H. *Inorg. Chem.* **1993**, *32*, 2212. (c) Shieh, M.; Liou, Y.; Jeng, B.-W. *Organometallics* **1993**, *12*, 4926. (d) Shieh, M.; Sheu, C.-m.; Ho, L.-F.; Cherng, J.-J.; Jang, L.-F.; Ueng, C.-H.; Peng, S.-M.; Lee, G.-H. *Inorg. Chem.* **1996**, *35*, 5504.

(6) (a) Shieh, M.; Chen, P.-F.; Peng, S.-M.; Lee, G.-H. *Inorg. Chem.* **1993**, *32*, 3389. (b) Shieh, M.; Tsai, Y.-C. *Inorg. Chem.* **1994**, *33*, 2303. (c) Shieh, M.; Shieh, M.-H.; Tsai, Y.-C.; Ueng, C.-H. *Inorg. Chem.* **1995**, *34*, 5088. (d) Shieh, M.; Tang, T.-F.; Peng, S.-M.; Lee, G.-H. *Inorg. Chem.* **1995**, *34*, 2797. (e) Shieh, M.; Tsai, Y.-C.; Cherng, J.-J.; Shieh, M.-H.; Chen, H.-S.; Ueng, C.-H. *Organometallics* **1997**, *16*, 456. (f) Cherng, J.-J.; Tsai, Y.-C.; Ueng, C.-H.; Lee, G.-H.; Peng, S.-M.; Shieh, M. *Organometallics* **1998**, *17*, 255. (g) Huang, K.-C.; Shieh, M.-H.; Jang, R.-J.; Peng, S.-M.; Lee, G.-H.; Shieh, M. *Organometallics* **1998**, *17*, 5202. (h) Shieh, M.; Chen, H.-S.; Chi, H.-H.; Ueng, C.-H. *Inorg. Chem.* **2000**, *39*, 5561. (i) Shieh, M.; Chen, H.-S.; Lai, Y.-W. *Organometallics* **2004**, *23*, 4018. (j) Lai, Y.-W.; Cherng, J.-J.; Sheu, W.-S.; Lee, G.-A.; Shieh, M. *Organometallics* **2006**, *25*, 184.

(7) Pfitzner, A. *Chem.—Eur. J.* **2000**, *6*, 1891.

(8) (a) Milazzo, G.; Caroli, S.; Sharma, V. K. *Tables of Standard Electrode Potentials*; Wiley: London, 1978. (b) Swift, E. H.; Butler, E. A. *Quantitative Measurements and Chemical Equilibria*; Freeman: New York, 1972. (c) Huemann, S.; Hai, N. T. M.; Broekmann, P.; Wandelt, K.; Zajonz, H.; Dosch, H.; Renner, F. *J. Phys. Chem. B* **2006**, *110*, 24955.

(9) (a) Łażewski, J.; Neumann, H.; Parlinski, K. *Phys. Rev B* **2004**, *70*, 195206. (b) Hamdadou, N.; Morsli, M.; Khelil, A.; Bernède, J. C. *J. Phys. D: Appl. Phys.* **2006**, *39*, 1042.

(10) (a) Bachman, R. E.; Whitmire, K. H. *Inorg. Chem.* **1994**, *33*, 2527. (b) Holliday, R. L.; Roof, L. C.; Hargus, B.; Smith, D. M.; Wood, P. T.; Pennington, W. T.; Kolis, J. W. *Inorg. Chem.* **1995**, *34*, 4392. (c) Konchenko, S. N.; Virovets, A. V.; Varnek, V. A.; Tkachev, S. V.; Podberezskaya, N. V.; Maksakov, V. A. *Zh. Strukt. Khim.* **1996**, *37*, 337.

Scheme 1

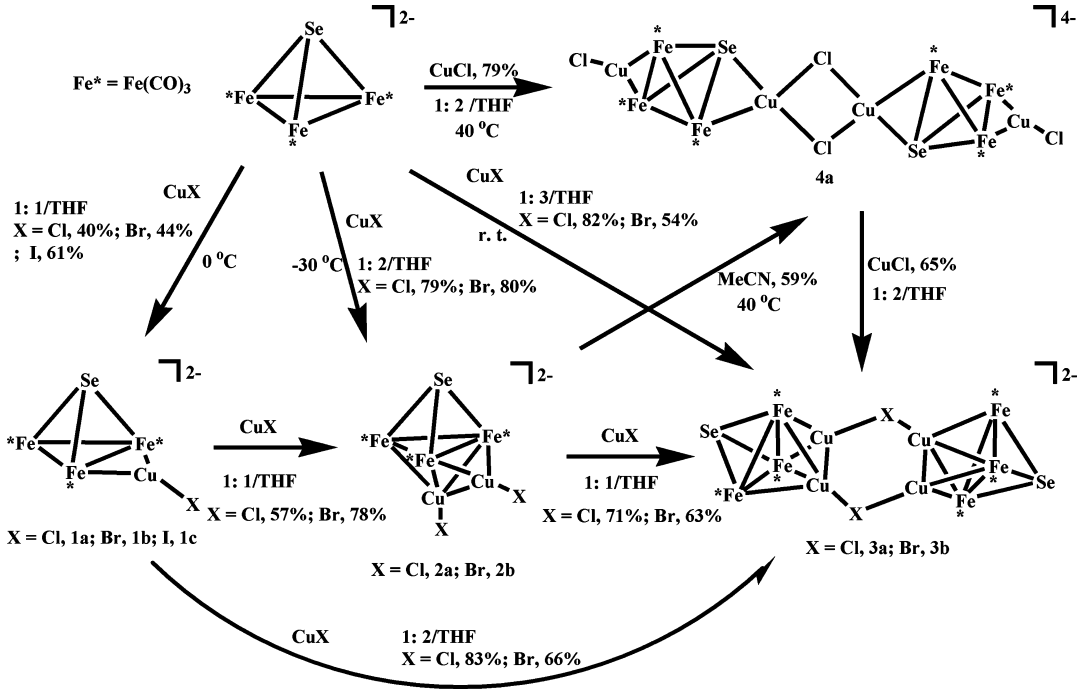

$[Et_4N]_2$[**3a**]; Br, $[PPh_4]_2$[**3b**]), respectively (Scheme 1). X-ray analysis showed that complexes **3a** and **3b** are isostructural species, each of which has a crystallographic center of symmetry at the center of the Cu_4X_2 ring (X = Cl, **3a**; Br, **3b**) (Figures 6,7) Complex **3a** and **3b** each consist of two $SeFe_3$ clusters asymmetrically linked by a Cu_4X_2 moiety (X = Cl, **3a**; Br, **3b**). It is interesting to note that complex **3a** contains a distorted Cu_4Cl_2 hexagon with the average distance of 0.248 Å to the least-squares plane while complex **3b** possesses an almost planar Cu_4Br_2 hexagon, suggestive of the size effect of the halide. Clusters **3a** and **3b** also can be viewed each to have two Se-capped Fe_3Cu_2 trigonal bipyramidal fragments which are further connected by two X atoms. In this regard, complex **3a** or **3b** can be considered as a dimer of cluster **2a** or **2b** by the elimination of 2 equiv of X^- (X = Cl, **3a**; Br, **3b**).

Reaction of $[Et_4N]_2[SeFe_3(CO)_9]$ with 2 equiv of CuCl at 40 °C. In contrast to the reaction at low temperatures (which formed $[Et_4N]_2$[**2a**]), the reaction of $[Et_4N]_2$-$[SeFe_3(CO)_9]$ with 2 equiv of CuCl in THF at 40 °C led to the isolation of the dimeric product of a $SeFe_3(CuCl)_2$ complex $[Et_4N]_4[\{SeFe_3(CO)_9(CuCl)_2\}_2]$ ($[Et_4N]_4$[**4a**]) in good yields (Scheme 1). Complex **4a** was shown by X-ray

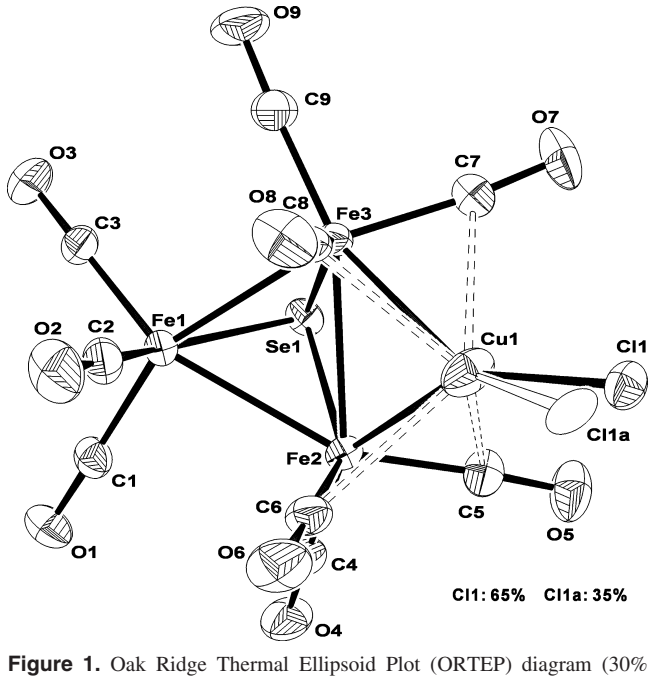

Figure 1. Oak Ridge Thermal Ellipsoid Plot (ORTEP) diagram (30% thermal ellipsoids) showing the structure and atom labeling for **1a**.

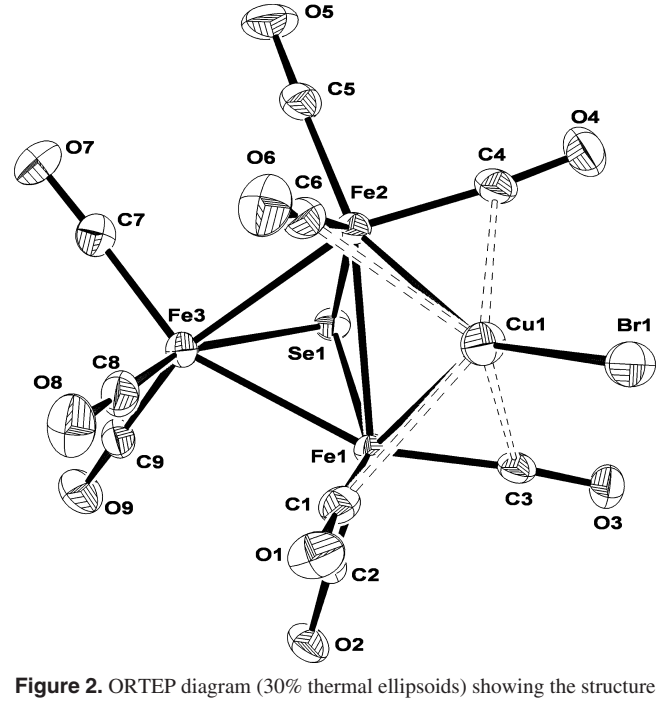

Figure 2. ORTEP diagram (30% thermal ellipsoids) showing the structure and atom labeling for **1b**.

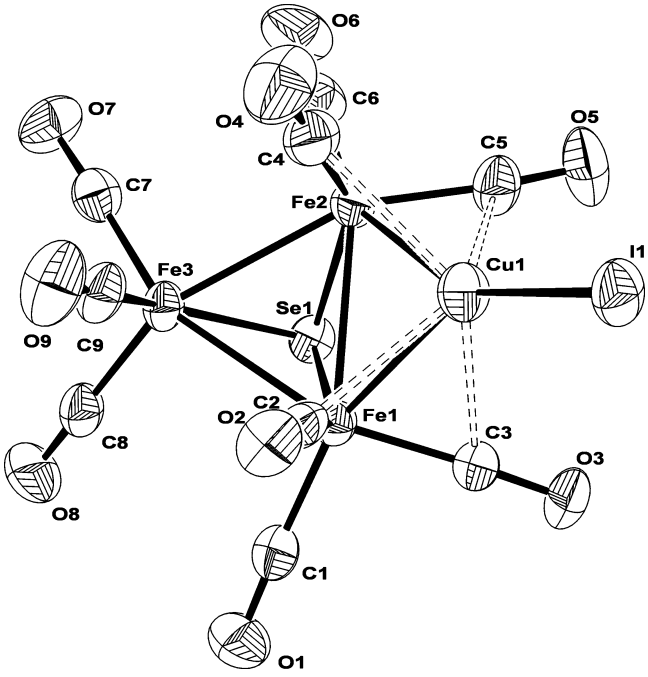

Figure 3. ORTEP diagram (30% thermal ellipsoids) showing the structure and atom labeling for **1c**.

analysis to have two asymmetric $SeFe_3CuCl$ clusters connected by two central Cu—Cl bonds, in which the Fe—Fe and Se—Fe edges of the $SeFe_3$ core each are bridged by one CuCl in the *trans* position (Figure 8). Hence, complex **4a** can be regarded as a Cu_2Cl_2-linked di-$SeFe_3CuCl$ cluster. As shown in Figure 8, two central Cu atoms each are coordinated to one Se, one Fe, and two bridging Cl atoms to give a nearly planar Cu_2Cl_2 ring, where the Cu atom is in the distorted planar coordination geometry (sum of angles: 382.1−382.9°).

Further, it was found that the kinetic product **2a** was not stable in solution and could gradually transform to its thermodynamic dimeric product **4a** in MeCN. The yield of the transformation at 40 °C was around 60% (Scheme 1). The formation of **4a** was confirmed by the IR spectra and the distinct XRD powder patterns of **2a** and **4a** in the solid state (Supporting Information, Figure S1). This conversion went smoothly in MeCN but not in THF because the higher polarity of MeCN helped to facilitate the formation of the highly charged complex **4a**. In addition, the large Coulomb attraction between cations and anions of $[Et_4N]_4$[**4a**] and significant hydrogen bonding interactions between hydrogen atoms of cations and Cl atoms of anions (C—Cl: 3.303−3.997 Å) in the crystal packing could also play important roles in its greater thermal stability.

Transformation among Complexes 1−4. Since varied ratios of $[Et_4N]_2[SeFe_3(CO)_9]$ and CuX under appropriate conditions lead to the formation of CuX- and Cu_2X_2-linked mono-$SeFe_3$-based complexes (**1a**, **1b**, **2a**, and **2b**) and Cu_4X_2- and Cu_2X_2-linked di-$SeFe_3$-based complexes (**3a**, **3b**, and **4a**), further examination of their rationalized transformation is of great interest in terms of the availability of the controlled stepwise construction of these ternary Se—Fe—Cu complexes. By carefully controlling ratios of the reactants and reaction conditions, the stepwise cluster-building processes of these Se—Fe—Cu clusters were accomplished (Scheme 1).

As shown in Scheme 1, it was found that CuX-incorporated $SeFe_3$ complexes **1a** and **1b** each could react with 1 equiv of CuX (X = Cl, Br) in THF to form the Cu_2X_2-incorporated $SeFe_3$ complexes **2a** or **2b**. Therefore, complexes **2a** and **2b** can be rationalized to result from the capping of CuX onto complexes **1a** and **1b** (X = Cl, Br), respectively. Besides, Cu_2X_2-incorporated $SeFe_3$ clusters **2a** and **2b** could further transform to Cu_4X_2-linked di-$SeFe_3$ clusters **3a** and **3b** in good yields, upon the addition of 1 equiv of CuX (X = Cl, Br). This result shows that the introduction of CuX into **2a** and **2b** facilitates the dimerization of **2a** and **2b** accompanied by the loss of 2 equiv of X^- (X = Cl, Br) to give **3a** and **3b**, respectively. By similar methodology, clusters **3a** and **3b** could be formed directly from **1a** and **1b** with 2 equiv of CuX (X = Cl, Br). In addition, it was found that the di-$SeFe_3$-based complex **4a** reacted with CuCl to cause the rearrangement of CuCl fragments accompanied with the release of Cl^- to give the di-$SeFe_3$-based cluster **3a**.

To understand better the formation of Cu_4X_2-linked di-$SeFe_3$ clusters **3a** and **3b** (X = Cl, Br) from Cu_2X_2-incorporated $SeFe_3$ clusters **2a** and **2b**, a detailed investigation was performed. The studies showed that the reaction of **2a** or **2b** with 1 equiv of CuX proceeded possibly via the formation of the proposed intermediate clusters $[SeFe_3(CO)_9(Cu_2X)]^-$ (X = Cl, **2a′**; Br, **2b′**), which were shown by Electrospray Ionization-Mass Spectrometry (ESI-MS) measurement immediately after the reaction mixture was mixed (ESI-MS (negative ion): $[M]^-$/e Calcd (Found): 661 (660.1), **2a′**; $[M]^-$/e Calcd (Found): 707 (706.2), **2b′** (Scheme 2). The formation of **2a′** from **2a** could be rationalized to result from the cleavage of the μ_4-Cu—Cl bond of **2a** because of the weaker μ_4-Cu—Cl bond versus the μ_3-Cu—Cl bond (2.194(3) vs 2.138(3) Å) by X-ray analysis. A similar phenomenon is also observed in **2b** (μ_4-Cu—Br bond vs the μ_3-Cu—Br bond (2.328(2) versus 2.259(2) Å). However, the argument that the observation of **2a′** and **2b′** in the ESI-MS measurement is due to the disintegration of the dimers **3a** and **3b** could not be completely excluded. To further support the existence of **2a′** and **2b′**, the reaction of **2a** and **2b** with 1 equiv of $AgNO_3$ was performed. It turned out that the reaction went quickly to form **3a** and **3b** with yields (∼60%) comparable to those with CuX. The function of CuX in the reaction of **2a** and **2b** to **3a** and **3b** was thought to be similar to that of $AgNO_3$ for the abstraction the weakly bounded X atoms of **2a** and **2b**. Therefore, it was proposed that **2a** or **2b** could readily lose the X^- upon the treatment of CuX to give the proposed intermediate **2a′** or **2b′** which would further undergo dimerization via the intermolecular attraction between Cu and X (X = Cl, Br) to give **3a** or **3b**, respectively. This hypothesis is further supported by DFT calculations (discussed later).

Furthermore, as listed in Table 1, it is found that the IR absorptions of the major CO bands of dianionic complexes **1**, **2**, and **3** are basically shifted to higher energies as the

Table 1. Experimental IR Data (cm^{-1}) for $[SeFe_3(CO)_9]^{2-}$, **1a**, **1b**, **1c**, **2a**, **2b**, **3a**, **3b**, and **4a**

complex		ν(CO) in THF, cm^{-1}
$[SeFe_3(CO)_9]^{2-}$		1996 (m), 1928 (vs), 1901 (s), 1872 (m)
$[SeFe_3(CO)_9CuX]^{2-}$	X = Cl, **1a**	2009 (w), 1951 (vs), 1921 (s), 1896 (w), 1879 (vw)
	X = Br, **1b**	2009 (w), 1950 (vs), 1917 (s), 1896 (w), 1875 (vw)
	X = I, **1c**	2010 (w), 1952 (vs), 1917 (s), 1900 (w), 1872 (vw)
$[SeFe_3(CO)_9Cu_2X_2]^{2-}$	X = Cl, **2a**	2024 (vw), 2009 (w), 1987 (m, sh), 1974 (s), 1961 (vs), 1915 (m), 1898 (w), 1879 (w)
	X = Br, **2b**	2025 (vw), 2010 (w), 1987 (m, sh), 1975 (s), 1961 (vs), 1917 (m), 1896 (w), 1879 (w)
$[\{SeFe_3(CO)_9\}_2Cu_4X_2]^{2-}$	X = Cl, **3a**	2024 (w), 1989 (vs), 1974 (s), 1941 (w), 1913 (m, br)
	X = Br, **3b**	2025 (w), 1989 (vs), 1975 (s), 1942 (w), 1913 (m, br)
$[\{SeFe_3(CO)_9(CuX)_2\}_2]^{4-}$	X = Cl, **4a**	2025 (vw), 2009 (w), 1975 (m, sh), 1962 (s), 1951 (vs), 1915 (m), 1897 (w), 1872 (w)

number of CuX or the size of the $SeFe_3$-based skeleton increased, which is related to the lower electron density in the Fe_3 ring back-transferred to the π^* orbitals of the carbonyls. In addition, the CO frequencies for the dimeric complex **4a** are similar but a bit shifted to low energies compared to those for its monomeric complex **2a**, probably because of the pronounced effect of the charge. It is more interesting to note that the size of clusters **1a**, **2a**, **3a**, and **4a** ranges from approximately 0.864, 0.897, 1.474, to 1.909 nm, which demonstrates the nanosized cluster growth of these ternary Se—Fe—Cu complexes.

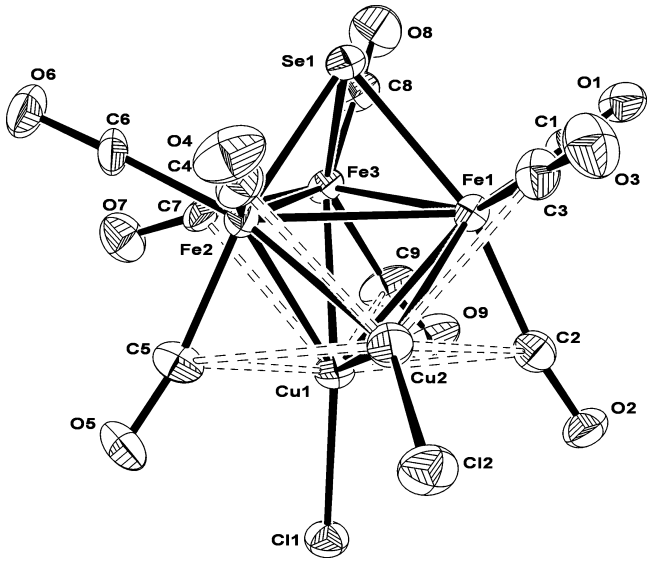

Figure 4. ORTEP diagram (30% thermal ellipsoids) showing the structure and atom labeling for **2a**.

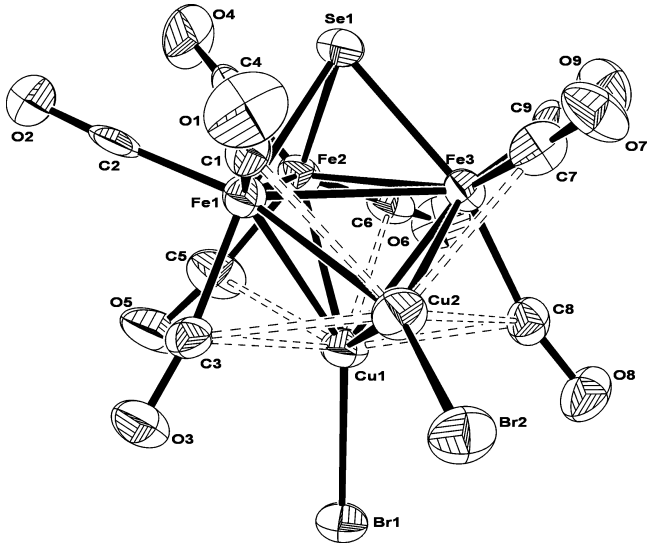

Figure 5. ORTEP diagram (30% thermal ellipsoids) showing the structure and atom labeling for **2b**.

X-ray Structural Comparison of $[Et_4N]_2$[1a], $[Et_4N]_2$[1b], $[Et_4N]_2$[1c], $[Et_4N]_2$[2a], $[Et_4N]_2$[2b], $[Et_4N]_2$[3a], $[PPh_4]_2$[3b], and $[Et_4N]_4$[4a]. According to the X-ray analysis, complexes **1a**−**1c**, **2a**, **2b**, **3a**, **3b**, and **4a** can be considered to exhibit the mono-$SeFe_3$- or di-$SeFe_3$-based core structures which are further linked by CuX, Cu_2X_2, or Cu_4X_2 (Figures 1−8). It is noted that **1a** exhibits a $SeFe_3$ core with one Fe—Fe edge bridged by one CuCl fragment in which the Cl(1) and Cl(1a) atoms are disordered and present in a 65:35 ratio (Figure 1). In addition, **2a** and **2b** each contain two independent but chemically similar asymmetric anions in the unit cell, which are similar in bond distances and angles and only one structure is described for comparison.

In terms of bonding modes of copper halides, the Fe—Fe bond of the $SeFe_3$ core of complexes **1a**−**1c** is bridged by μ_2-CuX, while the Fe_3 ring of the $SeFe_3$ core of complexes **2a** and **2b** is asymmetrically bridged by one μ_2-CuX and another μ_3-CuX with the two Cu atoms further bonded. While the di-$SeFe_3$ cluster **3** can be viewed as having two $SeFe_3$ cores linked by the μ_6-Cu_4X_2 ligand, the di-$SeFe_3$ cluster **4a** is regarded to have two μ_2-CuCl $SeFe_3$ cores linked by the μ_2-Cu_2Cl_2 fragment. It is noted that the bridging unit Cu_2Cl_2 in **4a** binds to the $SeFe_3$ core across the Se—Fe bond but not the Fe—Fe bond, which is unique in this Se—Fe—Cu carbonyl system and should be related to the reduction of the steric hindrance. Complexes **1a**−**1c** are structurally related to the previously reported H- or metal-bridged EFe_3 complexes (E = S, Se, Te) such as $[PPN][HSeFe_3(CO)_9]$,[11] $[SFe_3(CO)_9(AuPPh_3)]^-$,[12] $[Et_4N][SeFe_3(CO)_9HgI]$,[6e] $[PPN]_2[TeFe_3(CO)_9CuCl]$,[11] and $[PPh_4][TeFe_3(CO)_9(AuPPh_3)]$.[13] However, the Cu_2X_2 bonding mode of complexes **2a** and **2b** is rare and represents the first example in the chalcogen-iron carbonyl complexes. Similar bonding modes were found in the complexes with the bridging $AuPPh_3$ ligand,

(11) Bachman, R. E.; Whitmire, K. H.; van Hal, J. *Organometallics* **1995**, *14*, 1792.
(12) Albano, V. G.; Castellari, C.; Femoni, C.; Iapalucci, M. C.; Longoni, G.; Monari, M.; Rauccio, M.; Zacchini, S. *Inorg. Chim. Acta* **1999**, *291*, 372.
(13) Roof, L. C.; Smith, D. M.; Drake, G. W.; Pennington, W. T.; Kolis, J. W. *Inorg. Chem.* **1995**, *34*, 337.

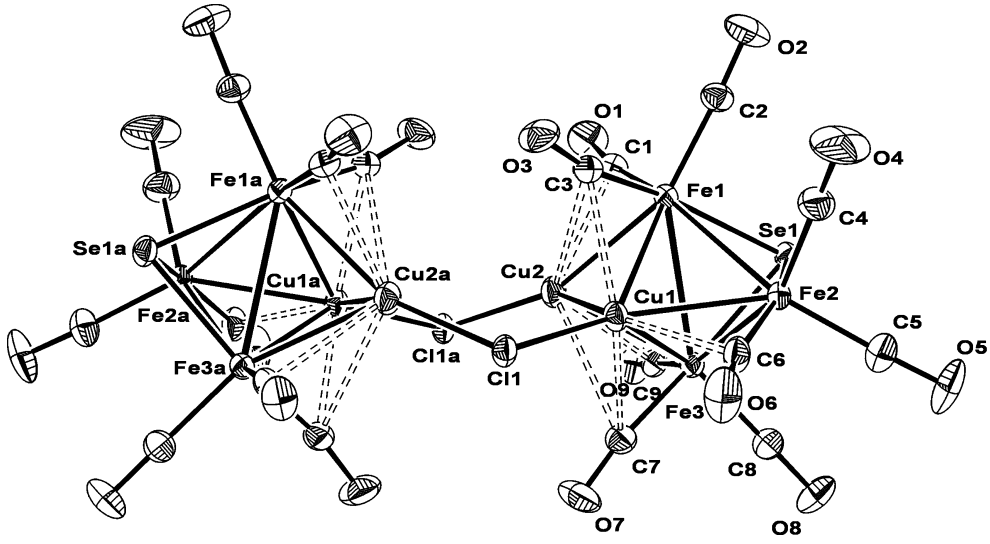

Figure 6. ORTEP diagram (30% thermal ellipsoids) showing the structure and atom labeling for **3a**.

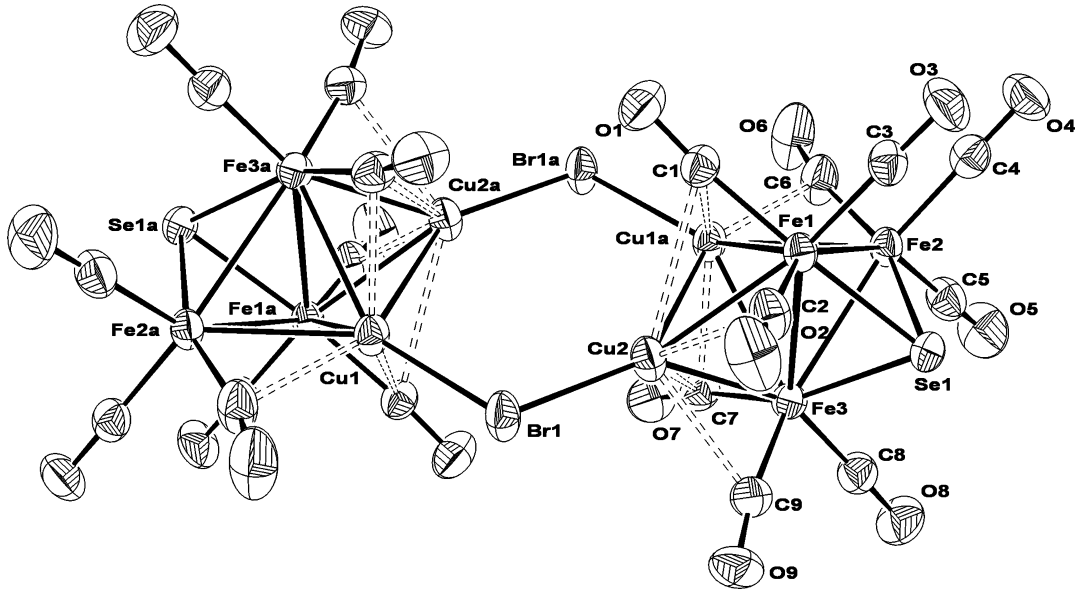

Figure 7. ORTEP diagram (30% thermal ellipsoids) showing the structure and atom labeling for **3b**.

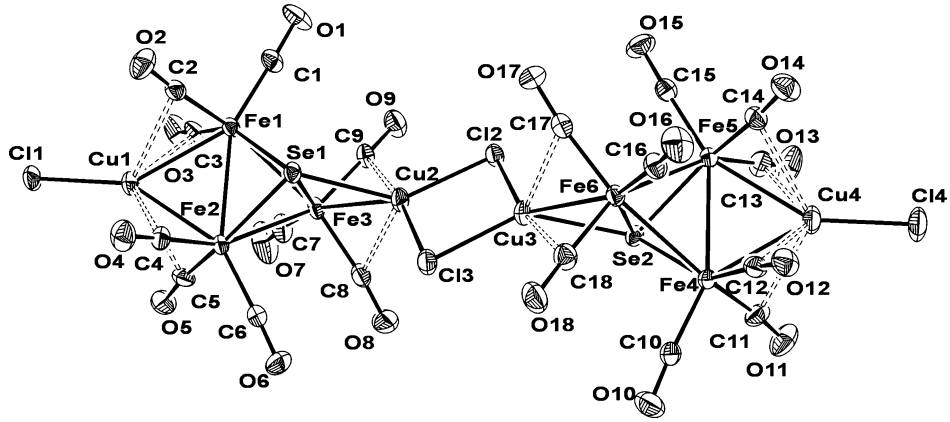

Figure 8. ORTEP diagram (30% thermal ellipsoids) showing the structure and atom labeling for **4a**.

$[EFe_3(CO)_9(AuPPh_3)_2]$[14,15] (E = O, S) and in the Ru-containing complexes with the bridging $CuPPh_3$ ligand.[16] In complexes **3a** and **3b**, two Cu—Cu bonds of the bridging unit Cu_4X_2 are equal (2.583(1), **3a**; 2.5930(7) Å, **3b**) and fall into the covalent bonding ranges while two X-bridged Cu···Cu distances are long (3.503(2), **3a**; 3.8246(6) Å, **3b**)

(14) Poliakova, L. A.; Gubin, S. P.; Belyakova, O. A.; Zubavichus, Y. V.; Slovokhotov, Y. L. *Organometallics* **1997**, *16*, 4527.

Scheme 2

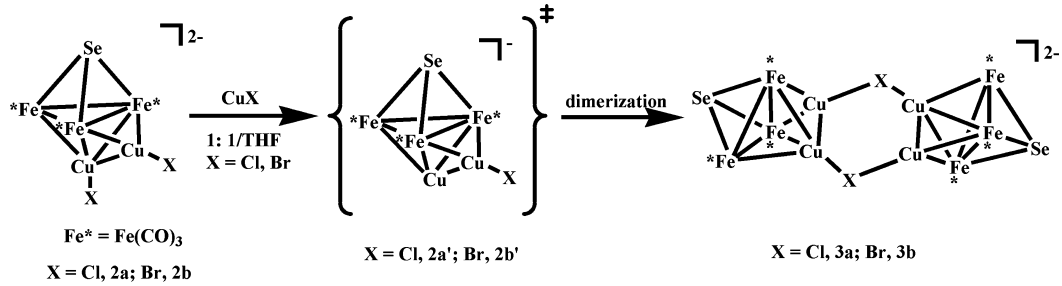

which are considered to be nonbonding. This bonding mode differs from the bridging Cu_4Cl_2 unit found in $[PPh_4]_2[\{TeRu_5(CO)_{14}\}_2Cu_4Cl_2]$[2e] and $[PPN]_2[\{Ru_6Cu_2C(CO)_{16}\}_2Cl_2]$,[17] where four Cu atoms are covalently bonded with two lengthening halide-bridged Cu—Cu bonds (ranging 2.779(1)−3.011(4) Å). The μ_2-Cu_2X_2 unit in **4a**, which binds to two Se and two Fe centers, can be comparable to the μ_4-Cu_2X_2 bonding in the cases of $[As_3MoCp^*(CO)_2(CuX)_2]_2$.[18] However, according to the CSD (Cambridge Structure Database) search, complex **4a** represents the rare examples of the Cu_2Cl_2 unit coordinated to both main group and transition metal atoms.[19]

Additionally, it is interesting to note that the bridging Cu atoms in these complexes interact with the carbon atoms of their neighboring CO ligands that adopt a weakly semibridging geometry. These Cu—C distances are within the van der Waals interaction (2.385(9)−2.509(9) Å, **1a**; 2.428(5)−2.499(5) Å, **1b**; 2.421(8)−2.510(9) Å, **1c**; 2.34(2)−3.08(1) Å, **2a**; 2.34(1)−3.02(2) Å, **2b**; 2.301(4)−2.916(4) Å, **3a**; 2.288(5)−2.856(5) Å, **3b**; 2.406(7)−2.819(7) Å, **4a**), and the corresponding Fe—C—O angles are slightly bent from 180° (173.2(8)−175.8(9)°, **1a**; 173.1(4)−176.5(4)°, **1b**; 170.7(7)−176.1(7)°, **1c**; 168.7(11)−174.9(12)°, **2a**; 167.0(12)−176.1(13)°, **2b**; 167.8(4)−176.0(3)°, **3a**; 167.4(4)−176.3(4)°, **3b**; 171.9(6)−176.2(5)°, **4a**) (See Figures 1−8).

Furthermore, for comparison, selected bond distances of these $SeFe_3$-based complexes and related complexes are listed in Table 2. As shown in Table 2, the corresponding Se—Fe, Fe—Fe, and Fe—Cu bond distances in these new Se—Fe—Cu complexes are generally similar and close to those found in the related complexes. However, the bridged Fe—Fe bond lengths in **1a**−**1c**, **2a**, **2b**, **3a**, **3b**, and **4a** are significantly longer than their unbridged Fe—Fe distances and the Fe—Fe bond in $[SeFe_3(CO)_9]^{2-}$ (2.620(7) Å), by virtue of the effect of bridging CuX fragments. Little halide effect on the length of the Fe—Fe and Fe—Cu bonds in **1a**−**1c**, **2a**−**2b**, and **3a**-**3b** was noted. Moreover, the lengthening of Cu—X bonds is noted as the metal skeleton, and the coordination number at the Cu atom increased from the mono-$SeFe_3$-based clusters (**1a**, **1b**, **2a**, and **2b**) to the di-$SeFe_3$-based clusters (**3a**, **3b**, and **4a**), which is in agreement with their Wiberg bond indices by DFT calculations. Finally, it is found that the dihedral angle of the Fe_3Cu butterfly in which the Cu atom bridges the Fe—Fe edge is different in these $SeFe_3$-based complexes. The dihedral angle in **2a**, **2b**, **3a**, **3b**, and **4a** (33.73(7), 34.63(8), 34.88(2), 35.31(2), 34.44(4)/38.15(4)°) becomes a bit smaller compared to those in **1a**−**1c** (36.11(6), 37.89(3), 39.60(5)°) as more CuX is introduced, which is also due to the increased coordination number of Cu atom or the size of metal skeleton.

DFT Computation. To further describe the electronic structures of clusters **1a**−**4a** and their relevant reactions, a hybrid density functional, B3LYP,[20,21] method with a modest basis set LanL2DZ was employed for computations. This level of calculation has been reported to work quite well for many charged inorganic and organometallic systems.[2e,6j,22] The geometries of complexes $[SeFe_3(CO)_9]^{2-}$, **1a**−**1c**, **2a**, **2b**, **3a**, **3b**, and **4a** were taken from single-crystal diffraction data, and the proposed intermediate **2a′** and **4a′** were fully optimized with the same level of theory. In addition, Wiberg bond indices[23] and natural population analyses (NPA)[24] for these complexes were also calculated and compared in Table 3.

As shown in Table 3, NPA for complexes **1a**−**4a** revealed that the Fe atoms in **1a**−**1c**, **2a**, **2b**, **3a**, **3b**, and **4a** each on average carried −0.37, −0.37, −0.37, −0.42, −0.44, −0.43, −0.42, and −0.38 charges while the Cu atoms in these

(15) (a) Roland, E.; Fischer, K.; Vahrenkamp, H. *Angew. Chem., Int. Ed. Engl.* **1983**, *22*, 326. (b) Fischer, K.; Deck, W.; Schwarz, M.; Vahrenkamp, H. *Chem. Ber.* **1985**, *118*, 4946.
(16) (a) Freeman, M. J.; Green, M.; Orpen, A. G.; Salter, I. D.; Stone, F. G. A. *Chem. Commun.* **1983**, 1332. (b) Freeman, M. J.; Orpen, A. G.; Salter, I. D. *J. Chem. Soc., Dalton Trans.* **1987**, 379.
(17) Beswick, M. A.; Lewis, J.; Raithby, P. R.; de Arellano, M. C. R. *J. Chem. Soc., Dalton Trans.* **1996**, 4033.
(18) Gregoriades, L. J.; Krauss, H.; Wachter, J.; Virovets, A. V.; Sierka, M.; Scheer, M. *Angew. Chem., Int. Ed.* **2006**, *45*, 4189.
(19) (a) Albano, V. G.; Busetto, L.; Cassani, M. C.; Sabatino, P.; Schmitz, A.; Zanotti, V. *J. Chem. Soc., Dalton Trans.* **1995**, 2087. (b) Pogrebnyakov, D. A.; Starikova, Z. A.; Pavlenko, N. I.; Rubailo, A. I.; Sokolenko, V. A.; Chudin, O. S.; Antonova, A. B. *Izv. Akad. Nauk SSSR, Ser. Khim.* **2002**, 1235.
(20) (a) Becke, A. D. *J. Chem. Phys.* **1993**, *98*, 5648. (b) Becke, A. D. *J. Chem. Phys.* **1992**, *96*, 2155. (c) Becke, A. D. *J. Chem. Phys.* **1992**, *97*, 9173.
(21) Lee, C.; Yang, W.; Parr, R. G. *Phys. Rev. B* **1988**, *37*, 785.
(22) (a) Goicoechea, J. M.; Hull, M. W.; Sevov, S. C. *J. Am. Chem. Soc.* **2007**, *129*, 7885. (b) Bengtsson-Kloo, L.; Iapalucci, C. M.; Longoni, G.; Ulvenlund, S. *Inorg. Chem.* **1998**, *37*, 4335. (c) Wong, K. M.-C.; Lam, S. C.-F.; Ko, C.-C.; Zhu, N.; Yam, V. W.-W.; Roué, S.; Lapinte, C.; Fathallah, S.; Costuas, K.; Kahlal, S.; Halet, J.-F. *Inorg. Chem.* **2003**, *42*, 7086. (d) Liu, C. W.; Lobana, T. S.; Xiao, J.-L.; Liu, H.-Y.; Liaw, B.-J.; Hung, C.-M.; Lin, Z. *Organometallics* **2005**, *24*, 4072. (e) Shieh, M.; Ho, L.-F.; Chen, P.-C.; Hsu, M.-H.; Chen, H.-L.; Guo, Y.-W.; Pan, Y.-W.; Lin, Y.-C. *Organometallics* **2007**, *26*, 6184. (f) Hsu, M.-H.; Chen, R.-T.; Sheu, W.-S.; Shieh, M. *Inorg. Chem.* **2006**, *45*, 6740.
(23) Wiberg, K. B. *Tetrahedron* **1968**, *24*, 1083.
(24) (a) Reed, A. E.; Weinhold, F. *J. Chem. Phys.* **1983**, *78*, 4066. (b) Reed, A. E.; Weinstock, R. B.; Weinhold, F. *J. Chem. Phys.* **1985**, *83*, 735.

Table 2. Average Bond Distance (Å) for **1a**, **1b**, **1c**, **2a**, **2b**, **3a**, **3b**, **4a**, and Related Complexes

complex	Se—Fe	Fe—Fe	Fe—Cu	Cu—X	Cu—Cu	Se—Cu	ref
$[SeFe_3(CO)_9]^{2-}$	2.302(4)	2.620(7)[b]					10c
1a	2.31(1)	2.610(4)[b] 2.688(1)[c]	2.489(8)	2.199(4)			*a*
1b	2.31(1)	2.614(2)[b] 2.6911(8)[c]	2.49(1)	2.2892(7)			*a*
1c	2.311(8)	2.612(5)[b] 2.700(2)[c]	2.49(1)	2.445(2)			*a*
2a	2.322(7)	2.70(6)[c]	2.55(6)	2.17(4)	2.691(2)[c]		*a*
2b	2.32(1)	2.70(7)[c]	2.55(7)	2.29(5)	2.682(2)[c]		*a*
3a	2.308(3)	2.72(7)[c]	2.52(2)	2.21(4)	2.583(1)[c] 3.503(2)[d]		*a*
3b	2.313(2)	2.72(5)[c]	2.54(2)	2.34(5)	2.5930(7)[c] 3.8246(6)[d]		*a*
4a	2.33(3)	2.621(5)[b] 2.679(8)[c]	2.52(3)	2.3(1)		2.41(1)	*a*
$[HSeFe_3(CO)_9]^-$	2.32(2)	2.615(8)[b] 2.689(3)[c]					11
$[SFe_3(CO)_9(AuPPh_3)]^-$		2.589(4)[b] 2.704(2)[c]					12
$[SeFe_3(CO)_9HgI]^-$	2.308(6)	2.620(6)[b] 2.887(3)[c]					6e
$[TeFe_3(CO)_9CuCl]^{2-}$		2.65(1)[b] 2.738(3)[c]	2.49(1)	2.150(4)			11
$[TeFe_3(CO)_9(AuPPh_3)]^-$		2.621(1)[b] 2.836(3)[c]					13
$[OFe_3(CO)_9(AuPPh_3)_2]$		2.61(9)[c]					14
$[SFe_3(CO)_9(AuPPh_3)_2]$		2.8(1)[c]					15
$[\{TeRu_5(CO)_{14}\}_2Cu_4Cl_2]^{2-}$				2.23(2)	2.608(1)[c] 2.779(1)[d]		2e
$[\{Ru_6Cu_2C(CO)_{16}\}_2Cl_2]^{2-}$				2.19(1)	2.677(3)[c] 3.011(4)[d]		17

[a] This work. [b] Unbridged. [c] Bridged by the metal fragment or H. [d] Bridged by Cl or Br atom.

Table 3. Results of Natural Bond Order (NBO) and NPA of $[SeFe_3(CO)_9]^{2-}$, **1a**, **1b**, **1c**, **2a**, **2b**, **3a**, **3b**, **4a**, and the Proposed Intermediates **2a′** and **4a′**

	Wiberg bond index						natural charge					
Complex	Se—Fe	Fe—Fe	Cu—Fe	Cu—X	Cu—Cu	Cu—Se	Se	Fe	Cu	X	$SeFe_3(CO)_9$ (sum)	Cu_mX_n (sum)
$[SeFe_3(CO)_9]^{2-}$ ($m = n = 0$)	0.42	0.16					−0.13	−0.39			−2	0
1a ($m = n = 1$)	0.46	0.21	0.08	0.29			−0.19	−0.37	0.67	−0.78	−1.90	−0.10
1b ($m = n = 1$)	0.46	0.21	0.08	0.30			−0.19	−0.37	0.64	−0.77	−1.87	−0.13
1c ($m = n = 1$)	0.46	0.21	0.08	0.32			−0.19	−0.37	0.61	−0.75	−1.86	−0.14
2a ($m = n = 2$)	0.47	0.21	0.08	0.28	0.04		−0.14	−0.42	0.63	−0.76	−1.74	−0.26
2b ($m = n = 2$)	0.47	0.20	0.08	0.29	0.04		−0.09	−0.44	0.60	−0.75	−1.70	−0.30
3a ($m = 4$, $n = 2$)	0.47	0.20	0.09	0.19	0.05		−0.10	−0.43	0.59	−0.68	−3.00	1.00
3b ($m = 4$, $n = 2$)	0.47	0.20	0.09	0.22	0.06		−0.08	−0.42	0.58	−0.64	−3.06	1.06
4a ($m = n = 4$)	0.43	0.21	0.07	0.21		0.18	−0.21	−0.38	0.69	−0.76	−3.71	−0.29
2a′ ($m = 2$, $n = 1$)	0.46	0.18	0.09	0.32	0.06		−0.09	−0.39	0.62	−0.74	−1.51	0.51
4a′ ($m = n = 2$)	0.41	0.20	0.08	0.33		0.19	−0.28	−0.35	0.66	−0.77	−1.79	−0.21

complexes had charges of +0.67, +0.64, +0.61, +0.63, +0.60, +0.59, +0.58, and +0.69, suggestive of some degree of ionic interaction between the Fe—Cu bonds. Their relevant Wiberg bond indices (0.08, **1a**; 0.08, **1b**; 0.08, **1c**; 0.08, **2a**; 0.08, **2b**; 0.09, **3a**; 0.09, **3b**; 0.07, **4a**) average 0.08, which is consistent with the weak ionic bonding between Fe and Cu in these complexes. It is noted that the Fe atoms linked to the Cu atom in complexes **1a**−**1c** are slightly more negatively charged than the Fe atom not involved probably because of the electron-withdrawing effect of CuX. Moreover, relatively greater Wiberg bond indices for the Se—Fe bonds in the $SeFe_3$ cores were found (0.46, **1a**; 0.46, **1b**; 0.46, **1c**; 0.47, **2a**; 0.47, **2b**; 0.47, **3a**; 0.47, **3b**; 0.43, **4a**), indicative of the stronger Se—Fe bonds, which should contribute to the stability of the $SeFe_3$ core in these CuX-incorporated $SeFe_3$-based frameworks. Therefore, the Se atom plays an important role in stabilizing the framework of these Se—Fe—Cu complexes. Further, as shown in Table 3, the computed natural charges for each $SeFe_3(CO)_9$ core

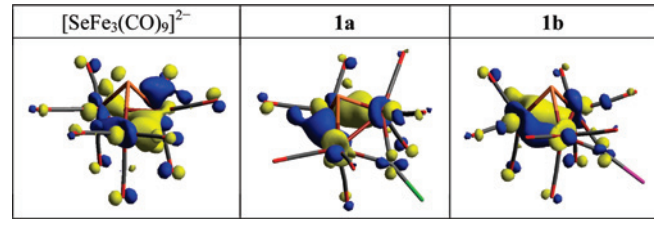

Figure 9. Spatial graphs (isovalue = 0.048) of the HOMO orbitals of $[SeFe_3(CO)_9]^{2-}$, **1a**, and **1b**.

in **1a**(**b**), **2a**(**b**), and **3a**(**b**) are decreasing in negative values, indicating the electron-withdrawing effect of the increased number of CuX or Cu.

Stepwise Formation of 1a−2b. Our calculated results revealed that the active sites for the stepwise formation of complexes **1a**−**1c** and **2a**−**2b** could be related to the electron density of the highest occupied molecular orbital (HOMO) of $[SeFe_3(CO)_9]^{2-}$ and **1a** or **1b**. As shown in Figure 9, the HOMO of $[SeFe_3(CO)_9]^{2-}$ has a significant contribution from the p and d orbitals of the Fe atoms. Hence, it is plausible

to suggest that the incoming CuX (X = Cl, Br, I) molecule could interact with the Fe atoms of $[SeFe_3(CO)_9]^{2-}$ to form new Fe—Cu bonds, giving rise to complexes **1a**−**1c**. It was also found that **1a** or **1b** can undergo a coupling reaction with 1 equiv of CuX to form complexes **2a** and **2b**, indicating that Fe and Cu centers of **1a** or **1b** are reactive sites for the electrophilic CuX, which is also supported by that the HOMO of **1a** or **1b** has a major contribution from the p and d orbitals of the Fe atoms and d orbitals of the Cu atom (Figure 9). As a consequence, it is reasonable to suggest that complexes **2a** and **2b** result from the capping of CuX onto the Fe_3Cu butterfly of the μ_2-CuX complexes **1a** and **1b** (X = Cl, Br), respectively.

Thermodynamic Feasibility of Dimerization. To further evaluate the validity of the transformation of the mono-$SeFe_3$-based complex **2a** to the di-$SeFe_3$-based complex **3a** or **4a**, without consideration of the vibrational and rotational contributions, a thermodynamic consideration of these reactions was carried out.

First, it is found that the reaction energies ΔE calculated by B3LYP and PW91PW91 levels for the reaction of mono-$SeFe_3$ **2a** with CuCl to form di-$SeFe_3$ complex **3a** are negative (−0.35 and −1.60 kcal/mol, respectively), which accounts for the formation of **3a** from **2a** and CuCl being favorable. For complex **2a**, the calculated Wiberg bond index of Cu(1)—Cl(1) is smaller than that for Cu(2)—Cl(2) (0.25 vs 0.30), which supports the cleavage of the μ_4-Cu(1)—Cl(1) bond of complex **2a** to form the proposed intermediate complex **2a′** (Scheme 2). Furthermore, the NPA calculation revealed that the Cu atoms in the proposed intermediate **2a′** carry +0.62 charge while the Cl atom carries −0.74 charge, which supports that the dimerization of the mono-$SeFe_3$ intermediate **2a′** to form the di-$SeFe_3$ complex **3a** proceeds via the significant intermolecular Coulomb interaction between the Cl and Cu atoms of two molecules of **2a′** (See Table 3).

Second, to understand the transformation of the kinetic product **2a** to its thermodynamic product **4a** at 40 °C, DFT calculations were performed on the basis of the X-ray determined geometries of complexes **2a** and **4a** in the gas-phase or in solutions (THF and MeCN). Our calculations show that the formation of di-$SeFe_3$ complex **4a** from the mono-$SeFe_3$ **2a** is unfavorable by 78.98 and 82.74 kcal/mol (B3LYP and PW91PW91 levels) in the gas-phase. However, this dimerization reaction turns out to be more favorable in both MeCN and THF solvents ($\Delta E = -26.69 \sim -18.85$ kcal/mol), which supports our experimental observations. On the basis of the structural features of **4a**, an isomeric mono-$SeFe_3$-based complex **4a′** was proposed to be an intermediate for the formation of **4a** (Scheme 3). The proposed intermediate **4a′** could be derived from the Cu—Cu and Fe—Cu bond breakage in complex **2a** based on their relatively weaker Wiberg bond indices (Table 3). To obtain more information, the optimized structure of the proposed intermediate **4a′** was calculated. It is found that two Cu atoms of **4a′** carry similar positive charges and two Cl atoms also carry similar negative charges, averaging +0.66 and −0.77, respectively (Table 3). Therefore, the dimerization of mono-$SeFe_3$ intermediate **4a′** to form di-$SeFe_3$ complex **4a** may occur via the significant intermolecular Coulomb interaction between the less hindrant Cu and Cl atoms (bridging Se—Fe bonds) in two molecules of **4a′**. On the basis of experimental and theoretical results, the negative charge and the less steric effect of the Se atom in the $SeFe_3$ core are both considered to play important roles in the formation of the thermal product **4a** which contains unique Cu-bridged Se—Fe bonds in this Se—Fe—Cu system.

Scheme 3

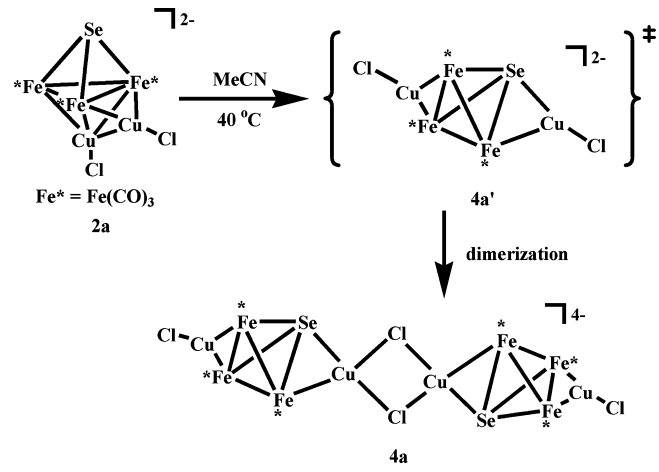

Electrochemistry. The electrochemical properties of $[SeFe_3(CO)_9]^{2-}$, **1a**−**1c**, **2b**, and **3b** in acetonitrile solution were investigated by cyclic voltammetry (CV) and differential pulse voltammetry (DPV) to study the effect of CuX on the $SeFe_3$ core. The electrochemical data of all the complexes studied are summarized in Supporting Information, Table S1.

As shown in Figure 10a, the CV study of the parent complex $[Et_4N]_2[SeFe_3(CO)_9]$ reveals one quasi-reversible redox couple at $E_{1/2} = -0.227$ V ($\Delta E = 95$ mV)[10b] and one irreversible reduction wave at −0.550 V. Further DPV study indicates that the quasi-reversible redox couple appears at −0.233 V with $W_{1/2} = 100$ mV (Figure 10b). In the CuX-incorporated system, the electrochemistry of $[Et_4N]_2$[**1a**], $[Et_4N]_2$[**1b**], $[Et_4N]_2$[**1c**], $[Et_4N]_2$[**2b**], and $[Et_4N]_2$[**3b**] shows some significant differences as compared to that of the parent complex $[Et_4N]_2[SeFe_3(CO)_9]$ (See Supporting Information, Table S1). Because of the interference of $[Et_4N]^+$, the scan range was set between +0.5 and −0.8 V. As shown in Figure 11a, **1b**, **2b**, and **3b** each show a sharp irreversible oxidation peak around $-0.35 \sim -0.28$ V in the CV scans because of the desorption of Cu;[25] however, other redox waves are somewhat broad and cannot be assigned unambiguously. Therefore, the DPV studies were carried out to explore their redox behavior between +0.4 to −0.8 V. Besides the Cu desorption at −0.345 V, the DPV studies further show that cluster **1b** displays one quasi-reversible oxida-

(25) (a) Xue, X.; Wang, X.-S.; Xiong, R.-G.; You, X.-Z.; Abrahams, B. F.; Che, C.-M.; Ju, H.-X. *Angew. Chem., Int. Ed.* **2002**, *41*, 2944. (b) Scheer, M.; Schindler, A.; Merkle, R.; Johnson, B. P.; Linseis, M.; Winter, R.; Anson, C. E.; Virovets, A. V. *J. Am. Chem. Soc.* **2007**, *129*, 13386. (c) Doescher, M. S.; Tour, J. M.; Rawlett, A. M.; Myrick, M. L. *J. Phys. Chem. B* **2001**, *105*, 105.

tion at 0.242 V ($W_{1/2}$ = 130 mV), one quasi-reversible reduction at −0.150 V ($W_{1/2}$ = 120 mV), and one irreversible reduction at −0.522 V (Figure 11b). The occurrence of the quasi-reversible oxidation at 0.242 V, which could not be observed in the parent complex $[Et_4N]_2[SeFe_3(CO)_9]$, is assignable to a one-electron redox at the Cu(I) center in the oxidation process. Compared to the reported redox potential at 0.23∼0.45 V for the Cu(I) center,[26] the relatively less positive potential at 0.242 V for **1b** is due to the electron-donating effect of the Fe_3 center. Similar redox waves (around 0.22∼0.28 V) for the Cu(I) center of complexes **1a**, **1c**, **2b**, and **3b** were also observed. More importantly, the quasi-reversible reduction at −0.150 V of **1b** in the reduction process conspicuously reveals a more anodic shift (80 mV) compared to that of $[SeFe_3(CO)_9]^{2-}$ (−0.233 V), attributed to the presence of the lower electron charge on the Fe_3 center owing to the electron-withdrawing effect of the CuBr fragment. Complexes **1a** and **1c** exhibit similar reduction potentials (around −0.14 ∼ −0.15 V) as **1b**, indicating small effect of halide. In addition, **2b** and **3b** also show the quasi-reversible reduction at −0.131 and −0.117 V with decreasing negative values compared to that for **1b** (−0.150 V), which is attributed to decreasing negative natural charges for each $SeFe_3(CO)_9$ core from **1b**, **2b**, to **3b** (see Table 3). Thus, the higher number of CuBr or Cu incorporated into the $SeFe_3$ core, the less negative potential for the quasi-reversible reduction it exhibits. This result is in contrast to the small effect of CuX found in the cases

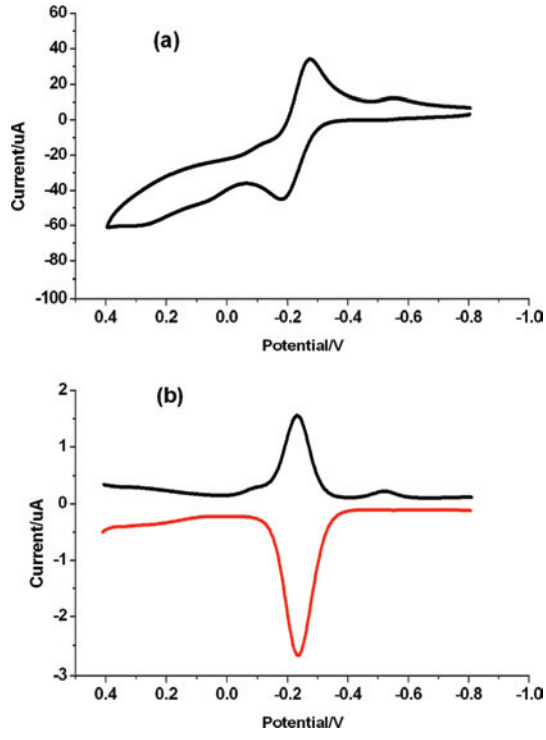

Figure 10. CVs (a) and DPVs (b) in MeCN for $[SeFe_3(CO)_9]^{2-}$. Conditions: electrolyte, 0.1 M Bu_4NClO_4; working electrode, glassy carbon; scan rate, 200 mV s^{-1}. Potentials are vs SCE.

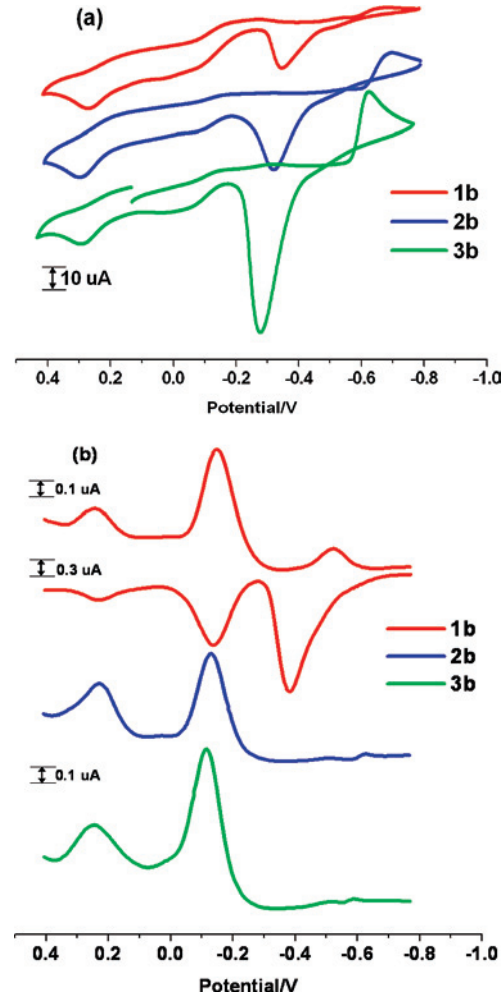

Figure 11. CVs (a) and DPVs (b) in MeCN for **1b**, **2b**, and **3b**. Conditions: electrolyte, 0.1 M Bu_4NClO_4; working electrode, glassy carbon; scan rate, 200 mV s^{-1}. Potentials are vs SCE.

Table 4. Reduction Potential, LUMO Energy Level, and Electronic Affinity of $[SeFe_3(CO)_9]^{2-}$, **1b**, **2b**, and **3b**

compound	reduction potential E^a (V)	LUMO (a.u.)	EA[b] (kcal/mol)
$[SeFe_3(CO)_9]^{2-}$	−0.233	0.15326	121.32
1b	−0.150	0.14564	114.03
2b	−0.131	0.11435	94.26
3b	−0.117	0.07214	64.86

[a] From differential pulse voltammetry. [b] The EA can be estimated by EA ≈ $E_{elec}(N+1) - E_{elec}(N)$ where $E_{elec}(N+1)$ and $E_{elec}(N)$ represent the electronic energies of molecules with $N+1$ and N electrons, respectively.

of ferrocene-based complexes.[27] As listed in Table 4, the decreasing quasi-reversible reduction potential for **1b**, **2b**, and **3b** is also consistent with the calculated trend for their lowest unoccupied molecular orbital (LUMO) energy level and electronic affinity. Further, the irreversible reduction peaks around −0.50 ∼ −0.63 V for **1a**−**1c**, **2b**, and **3b** were measured by the DPV study (the relative peaks can not be distinguishable in CV), which is attributable to the

(26) (a) Yam, V. W.-W.; Lee, W.-K.; Lai, T.-F. *Organometallics* **1993**, *12*, 2383. (b) Yam, V. W.-W.; Lee, W.-K.; Cheung, K.-K.; Crystall, B.; Phillips, D. *J. Chem. Soc., Dalton Trans.* **1996**, 3283. (c) Yam, V. W.-W.; Fung, W. K.-M.; Wong, M.-T. *Organometallics* **1997**, *16*, 1772. (d) Yam, V. W.-W.; Fung, W. K.-M.; Cheung, K.-K. *Organometallics* **1998**, *17*, 3293.
(27) Horikoshi, R.; Ueda, M.; Mochida, T. *New J. Chem.* **2003**, *27*, 933.

irreversible reduction of $[SeFe_3(CO)_9]^{2-}$ core and the irreversible reduction of the Cu(I) center.[25]

Conclusion

In this study, a new series of CuX-, Cu_2X_2-, and Cu_4X_2-incorporated mono- or di-$SeFe_3$-based clusters has been synthesized from the reaction of $[SeFe_3(CO)_9]^{2-}$ with CuX (X = Cl, Br) in appropriate ratios. The stepwise cluster growth can be achieved from CuX-incorporated to Cu_2X_2-incorporated mono-$SeFe_3$ complexes or to Cu_2X_2-linked di-$SeFe_3$-based complexes, and further to Cu_4X_2-linked complexes, depending on the amount of CuX added and reaction conditions. The electrochemical study shows the significant anodic shift of the CuX-incorporated $SeFe_3$ complexes compared with the parent $SeFe_3$-cluster, indicative of the pronounced electronic effect of CuX on the $SeFe_3$ core. In addition, the nature, formation, and electrochemistry of the resultant complexes are fully understood by molecular calculations at the B3LYP level of the DFT in terms of the effects of selenium, iron, copper halides, and the size of the metal skeleton. This study paves a new avenue to the controllable stepwise construction of Se—Fe—Cu carbonyl clusters from the viewpoints of both synthetic and theoretical applications.

Experimental Section

All reactions were performed under an atmosphere of pure nitrogen using standard Schlenk techniques.[28] Solvents were purified, dried, and distilled under nitrogen prior to use. CuCl (Aldrich), CuBr (Aldrich), and CuI (Aldrich) were used as received. $[Et_4N]_2[SeFe_3(CO)_9]$ was prepared according to the published method.[6b] Infrared spectra were recorded on a Perkin-Elmer Paragon 500 IR spectrometer as solutions in CaF_2 cells. Elemental analyses of C, H, and N were performed on a Perkin-Elmer 2400 analyzer at the NSC Regional Instrumental Center at National Taiwan University, Taipei, Taiwan. Powder XRD data were recorded on a Bruker D8 ADVANCE instrument at 40 kV and 40 mA with $Cu_{K\alpha}$ radiation (λ = 1.54050 Å). ESI-MS spectra were obtained on a Thermo Finnigan LCQ Advantage mass spectrometer.

Synthesis of $[Et_4N]_2[SeFe_3(CO)_9CuCl]$ ($[Et_4N]_2$[1a]). THF (20 mL) was added to a mixture of $[Et_4N]_2[SeFe_3(CO)_9]$ (0.51 g, 0.67 mmol) and CuCl (0.06 g, 0.61 mmol) in an ice−water bath. The mixture was stirred in an ice−water bath for 10 min to give a reddish-brown solution, which was filtered, and the solvent was removed under vacuum. The residue was then washed with Hexanes and Et_2O several times. The THF extract was recrystallized with Et_2O/MeOH/THF to give a reddish-brown sample of $[Et_4N]_2[SeFe_3(CO)_9CuCl]$ ($[Et_4N]_2$[**1a**]) (yield 0.21 g, 40%). IR (THF): ν_{CO} = 2009 (w), 1951 (vs), 1921 (s), 1896 (w), 1879 (vw) cm^{-1}. Anal. Calcd for $C_{25}H_{40}ClCuFe_3N_2O_9Se$: C, 34.99; H, 4.70; N, 3.26. Found: C, 34.63; H, 4.65; N, 3.22. Crystals of $[Et_4N]_2$[**1a**] suitable for XRD were grown from Et_2O/MeOH/THF.

Synthesis of $[Et_4N]_2[SeFe_3(CO)_9CuBr]$ ($[Et_4N]_2$[1b]). THF (20 mL) was added to a mixture of $[Et_4N]_2[SeFe_3(CO)_9]$ (0.50 g, 0.66 mmol) and CuBr (0.09 g, 0.63 mmol) in an ice−water bath. The mixture was stirred in an ice−water bath for 10 min to give a reddish-brown solution, which was filtered, and the solvent was removed under vacuum. The residue was then washed several times with Hexanes and Et_2O. The THF extract was recrystallized with Et_2O/MeOH/THF to give a reddish-brown sample of $[Et_4N]_2[SeFe_3(CO)_9CuBr]$ ($[Et_4N]_2$[**1b**]) (yield 0.25 g, 44%). IR (THF): ν_{CO} = 2009 (w), 1950 (vs), 1917 (s), 1896 (w), 1875 (vw) cm^{-1}. Anal. Calcd for $C_{25}H_{40}BrCuFe_3N_2O_9Se$: C, 33.27; H, 4.47; N, 3.10. Found: C, 33.06; H, 4.35; N, 3.28. Crystals of $[Et_4N]_2$[**1b**] suitable for XRD were grown from Et_2O/MeOH/THF.

Synthesis of $[Et_4N]_2[SeFe_3(CO)_9CuI]$ ($[Et_4N]_2$[1c]). THF (20 mL) was added to a mixture of $[Et_4N]_2[SeFe_3(CO)_9]$ (0.50 g, 0.66 mmol) and CuI (0.13 g, 0.68 mmol) in an ice−water bath. The mixture was stirred in an ice−water bath for 10 min to give a reddish-brown solution, which was filtered, and the solvent was removed under vacuum. The residue was then washed several times with Hexanes and Et_2O. The THF extract was recrystallized with Et_2O/MeOH/THF to give a reddish-brown sample of $[Et_4N]_2[SeFe_3(CO)_9CuI]$ ($[Et_4N]_2$[**1c**]) (yield 0.38 g, 61%). IR (THF): ν_{CO} = 2010 (w), 1952 (vs), 1917 (s), 1900 (w), 1872 (vw) cm^{-1}. Anal. Calcd for $C_{25}H_{40}ICuFe_3N_2O_9Se$: C, 31.62; H, 4.25; N, 2.95. Found: C, 31.67; H, 4.26; N, 2.80. Crystals of $[Et_4N]_2$[**1c**] suitable for XRD were grown from Et_2O/MeOH/THF.

Synthesis of $[Et_4N]_2[SeFe_3(CO)_9Cu_2Cl_2]$ ($[Et_4N]_2$[2a]). THF (7.5 mL) was added to a mixture of $[Et_4N]_2[SeFe_3(CO)_9]$ (0.38 g, 0.50 mmol) and CuCl (0.10 g, 1.00 mmol). The mixture was stirred at −30 °C for 10 min to give a reddish-brown solution, which was filtered, and the solvent was removed under vacuum. The THF extract was recrystallized with Et_2O/THF to give a reddish-brown sample of $[Et_4N]_2[SeFe_3(CO)_9Cu_2Cl_2]$ ($[Et_4N]_2$[**2a**]) (yield 0.38 g, 79%). The XRD pattern of $[Et_4N]_2$[**2a**] was in agreement with that calculated from single crystal XRD. IR (THF): ν_{CO} = 2024 (vw), 2009 (w), 1987(m, sh), 1974 (s), 1961 (vs), 1915 (m), 1898 (w), 1879 (w) cm^{-1}. Anal. Calcd for $C_{25}H_{40}Cl_2Cu_2Fe_3N_2O_9Se$: C, 31.37; H, 4.21; N, 2.93. Found: C, 31.47; H, 4.34; N, 2.82. Crystals of $[Et_4N]_2$[**2a**] suitable for XRD were grown from Et_2O/THF at −30 °C.

Synthesis of $[Et_4N]_2[SeFe_3(CO)_9Cu_2Br_2]$ ($[Et_4N]_2$[2b]). THF (10 mL) was added to a mixture of $[Et_4N]_2[SeFe_3(CO)_9]$ (0.38 g, 0.50 mmol) and CuBr (0.15 g, 1.05 mmol). The mixture was stirred at −30 °C for 5 min to give a reddish-brown solution, which was filtered, and the solvent was removed under vacuum. The THF extract was recrystallized with Et_2O/THF to give a reddish-brown sample of $[Et_4N]_2[SeFe_3(CO)_9Cu_2Br_2]$ ($[Et_4N]_2$[**2b**]) (yield 0.42 g, 80%). The XRD pattern of $[Et_4N]_2$[**2b**] was in agreement with that calculated from single crystal XRD. IR (THF): ν_{CO} = 2025 (vw), 2010 (w), 1987 (m, sh), 1975 (s), 1961 (vs), 1917 (m), 1896 (w), 1879 (w) cm^{-1}. Anal. Calcd for $C_{25}H_{40}Br_2Cu_2Fe_3N_2O_9Se$: C, 28.71; H, 3.85; N, 2.68. Found: C, 29.04; H, 3.91; N, 2.65. Crystals of $[Et_4N]_2$[**2b**] suitable for XRD were grown from Et_2O/THF at −30 °C.

Synthesis of $[Et_4N]_2[\{SeFe_3(CO)_9\}_2Cu_4Cl_2]$ ($[Et_4N]_2$[3a]). THF (7.5 mL) was added to a mixture of $[Et_4N]_2[SeFe_3(CO)_9]$ (0.15 g, 0.20 mmol) and CuCl (0.06 g, 0.61 mmol). The mixture was stirred at room temperature for 40 min to give a purplish-brown solution, which was filtered, and the solvent was removed under vacuum. The THF extract was recrystallized with Et_2O/MeOH/THF to give a purplish-brown sample of $[Et_4N]_2[\{SeFe_3(CO)_9\}_2Cu_4Cl_2]$ ($[Et_4N]_2$[**3a**]) (yield 0.13 g, 82%). IR (THF): ν_{CO} = 2024 (w), 1989 (vs), 1974 (s), 1941 (w), 1913 (m, br) cm^{-1}. Anal. Calcd for $C_{34}H_{40}Cl_2Cu_4Fe_6N_2O_{18}Se_2$: C, 25.80; H, 2.55; N, 1.77. Found: C, 26.15; H, 2.63; N, 1.92. Crystals of $[Et_4N]_2$[**3a**] suitable for XRD were grown from Et_2O/THF.

Synthesis of $[Et_4N]_2[\{SeFe_3(CO)_9\}_2Cu_4Br_2]$ ($[Et_4N]_2$[3b]). THF (7 mL) was added to a mixture of $[Et_4N]_2[SeFe_3(CO)_9]$ (0.15 g, 0.20 mmol) and CuBr (0.09 g, 0.63 mmol) in an ice−water bath.

(28) Shriver, D. F.; Drezdon, M. A. *The Manipulation of Air-Sensitive Compounds*; Wiley-VCH Publishers: New York, 1986.

The mixture was stirred in an ice−water bath for 40 min to give a purplish-brown solution, which was filtered, and the solvent was removed under vacuum. The THF extract was recrystallized with Et_2O/MeOH/THF to give a purplish-brown sample of $[Et_4N]_2[\{SeFe_3(CO)_9\}_2Cu_4Br_2]$ ($[Et_4N]_2$[**3b**]) (yield 0.09 g, 54%). IR (THF): ν_{CO} = 2025 (w), 1989 (vs), 1975 (s), 1942 (w), 1913 (m, br) cm^{-1}. Anal. Calcd for $C_{34}H_{40}Br_2Cu_4Fe_6O_{18}N_2Se_2$: C, 24.43; H, 2.41; N, 1.68. Found: C, 24.78; H, 2.75; N, 1.96. $[PPh_4]_2$[**3b**] was prepared with similar procedures. Crystals of $[PPh_4]_2$[**3b**] suitable for XRD were grown from Et_2O/MeOH/THF.

Synthesis of $[Et_4N]_4[\{SeFe_3(CO)_9(CuCl)_2\}_2]$ ($[Et_4N]_4$[4a]). THF (20 mL) was added to a mixture of $[Et_4N]_2[SeFe_3(CO)_9]$ (0.38 g, 0.50 mmol) and CuCl (0.10 g, 1.00 mmol). The mixture was heated at 40 °C for 10 min to give a reddish-brown solution, which was filtered, and the solvent was removed under vacuum. The THF extract was recrystallized with Et_2O/THF to give a reddish-brown sample of $[Et_4N]_4[\{SeFe_3(CO)_9(CuCl)_2\}_2]$ ($[Et_4N]_4$[**4a**]) (yield 0.38 g, 79%). IR (THF): ν_{CO} = 2025 (vw), 2009 (w), 1975 (m, sh), 1962 (s), 1951 (vs), 1915 (m), 1897 (w), 1872 (w) cm^{-1}. Anal. Calcd for $C_{50}H_{80}Cl_4Cu_4Fe_6N_4O_{18}Se_2$: C, 31.37; H, 4.21; N, 2.93. Found: C, 31.22; H, 3.89; N, 2.69. Crystals of $[Et_4N]_4$[**4a**] suitable for XRD were grown from Et_2O/MeOH/THF.

Conversion of $[Et_4N]_2$[1a] to $[Et_4N]_2$[2a]. THF (5 mL) was added to a mixture of $[Et_4N]_2$[**1a**] (0.17 g, 0.20 mmol) and CuCl (0.02 g, 0.20 mmol). The mixture was stirred at −30 °C for 10 min to give a reddish-brown solution, which was filtered, and the solvent was removed under vacuum. The THF extract was recrystallized with Et_2O/THF to give a reddish-brown sample of $[Et_4N]_2[SeFe_3(CO)_9(CuCl)_2]$ ($[Et_4N]_2$[**2a**]) (yield 0.11 g, 57%).

Conversion of $[Et_4N]_2$[1b] to $[Et_4N]_2$[2b]. THF (10 mL) was added to a mixture of $[Et_4N]_2$[**1b**] (0.36 g, 0.40 mmol) and CuBr (0.06 g, 0.42 mmol). The mixture was stirred −30 °C for 30 min to give a reddish-brown solution, which was filtered, and the solvent was removed under vacuum. The THF extract was recrystallized with Et_2O/THF to give a reddish-brown sample of $[Et_4N]_2[SeFe_3(CO)_9(CuBr)_2]$ ($[Et_4N]_2$[**2b**]) (yield 0.32 g, 78%).

Conversion of $[Et_4N]_2$[2a] to $[Et_4N]_2$[3a]. Method A. THF (10 mL) was added to a mixture of $[Et_4N]_2$[**2a**] (0.29 g, 0.30 mmol) and CuCl (0.03 g, 0.30 mmol). The mixture was stirred at room temperature for 30 min to give a reddish-brown solution, which was filtered, and the solvent was removed under vacuum. The THF extract was recrystallized with Et_2O/MeOH/THF to give a reddish-brown sample of $[Et_4N]_2[\{SeFe_3(CO)_9\}_2Cu_4Cl_2]$ ($[Et_4N]_2$[3a]) (yield 0.17 g, 71%).

Method B. THF (10 mL) was added to a mixture of $[Et_4N]_2$[**2a**] (0.14 g, 0.15 mmol) and $AgNO_3$ (0.03 g, 0.18 mmol). The mixture was stirred at 0 °C for 50 min to give a reddish-brown solution, which was filtered, and the solvent was removed under vacuum. The THF extract was recrystallized with Et_2O/MeOH/THF to give a reddish-brown sample of $[Et_4N]_2[\{SeFe_3(CO)_9\}_2Cu_4Cl_2]$ ($[Et_4N]_2$[3a]) (yield 0.07 g, 60%).

Conversion of $[Et_4N]_2$[2b] to $[Et_4N]_2$[3b]. Method A. THF (7 mL) was added to a mixture of $[Et_4N]_2$[**2b**] (0.18 g, 0.17 mmol) and CuBr (0.03 g, 0.21 mmol) in an ice−water bath. The mixture was stirred in an ice−water bath for 30 min to give a reddish-brown solution that was filtered, and the solvent was removed under vacuum. The THF extract was recrystallized with Et_2O/MeOH/THF to give a reddish-brown sample of $[Et_4N]_2[\{SeFe_3(CO)_9\}_2Cu_4Br_2]$ ($[Et_4N]_2$[**3b**]) (yield 0.09 g, 63%).

Method B. THF (10 mL) was added to a mixture of $[Et_4N]_2$[**2b**] (0.24 g, 0.23 mmol) and $AgNO_3$ (0.04 g, 0.24 mmol). The mixture was stirred at 0 °C for 50 min to give a reddish-brown solution, which was filtered, and the solvent was removed under vacuum. The THF extract was recrystallized with Et_2O/MeOH/THF to give a reddish-brown sample of $[Et_4N]_2[\{SeFe_3(CO)_9\}_2Cu_4Br_2]$ ($[Et_4N]_2$[**3b**]) (yield 0.10 g, 52%).

Conversion of $[Et_4N]_2$[1a] to $[Et_4N]_2$[3a]. THF (10 mL) was added to a mixture of $[Et_4N]_2$[**1a**] (0.17 g, 0.20 mmol) and CuCl (0.04 g, 0.40 mmol). The mixture was stirred at room temperature for 30 min to give a reddish-brown solution, which was filtered, and the solvent was removed under vacuum. The THF extract was recrystallized with Et_2O/MeOH/THF to give a reddish-brown sample of $[Et_4N]_2[\{SeFe_3(CO)_9\}_2Cu_4Cl_2]$ ($[Et_4N]_2$[**3a**]) (yield 0.13 g, 83%).

Conversion of $[Et_4N]_2$[1b] to $[Et_4N]_2$[3b]. THF (7.5 mL) was added to a mixture of $[Et_4N]_2$[**1b**] (0.28 g, 0.31 mmol) and CuBr (0.09 g, 0.63 mmol). The mixture was stirred at 0 °C for 40 min to give a reddish-brown solution, which was filtered, and the solvent was removed under vacuum. The THF extract was recrystallized with Et_2O/MeOH/THF to give a reddish-brown sample of $[Et_4N]_2[\{SeFe_3(CO)_9\}_2Cu_4Br_2]$ ($[Et_4N]_2$[**3b**]) (yield 0.17 g, 66%).

Conversion of $[Et_4N]_2$[2a] to $[Et_4N]_4$[4a]. MeCN (20 mL) was added to 0.41 g (0.43 mmol) of $[Et_4N]_2$[**2a**]. The resulting solution was heated at 40 °C for 1 h to give a reddish-brown solution, which was filtered, and the solvent was removed under vacuum. The MeCN extract was recrystallized with Et_2O/MeOH/MeCN to give a reddish-brown sample of $[Et_4N]_4[\{SeFe_3(CO)_9(CuCl)_2\}_2]$ ($[Et_4N]_4$[**4a**]) (yield 0.24 g, 59%).

Conversion of $[Et_4N]_4$[4a] to $[Et_4N]_2$[3a]. THF (20 mL) was added to a mixture of $[Et_4N]_4$[**4a**] (0.57 g, 0.30 mmol) and CuCl (0.06 g, 0.61 mmol). The mixture was stirred at room temperature for 30 min to give a reddish-brown solution, which was filtered, and the solvent was removed under vacuum. The THF extract was recrystallized with Et_2O/THF to give a reddish-brown sample of $[Et_4N]_2[\{SeFe_3(CO)_9\}_2Cu_4Cl_2]$ ($[Et_4N]_2$[**3a**]) (yield 0.31 g, 65%).

X-ray Structural Characterization of $[Et_4N]_2$[1a], $[Et_4N]_2$[1b], $[Et_4N]_2$[1c], $[Et_4N]_2$[2a], $[Et_4N]_2$[2b], $[Et_4N]_2$[3a], $[PPh_4]_2$[3b], and $[Et_4N]_4$[4a]. The selected crystallographic data for $[Et_4N]_2$[**1a**], $[Et_4N]_2$[**1b**], $[Et_4N]_2$[**1c**], $[Et_4N]_2$[**2a**], $[Et_4N]_2$[**2b**], $[Et_4N]_2$[**3a**], $[PPh_4]_2$[**3b**], $[Et_4N]_4$[**4a**] are given in Table 5. All crystals were mounted on glass fibers with epoxy cement. Data collection for $[Et_4N]_2$[**1a**], $[Et_4N]_2$[**1b**], $[Et_4N]_2$[**2a**], $[PPh_4]_2$[**3b**], and $[Et_4N]_4$[**4a**] was carried out on a Bruker Nonius Kappa CCD diffractometer using graphite-monochromated $Mo_{K\alpha}$ radiation, and an empirical absorption correction by multiscan was applied.[29] Data collection for $[Et_4N]_2$[**1c**], $[Et_4N]_2$[**2b**], and $[Et_4N]_2$[**3a**] was carried out on a Nonius (CAD-4) diffractometer using graphite-monochromated $Mo_{K\alpha}$ radiation employing the $\theta-2\theta$ scan mode, and an empirical absorption correction by ψ-scans was applied.[30] The structures were solved by direct methods and were refined with SHELXL-97.[31] All of the non-hydrogen atoms were refined with anisotropic temperature factors. The selected distances and angles for $[Et_4N]_2$[**1a**], $[Et_4N]_2$[**1b**], $[Et_4N]_2$[**1c**], $[Et_4N]_2$[**2a**], $[Et_4N]_2$[**2b**], $[Et_4N]_2$[**3a**], $[PPh_4]_2$[**3b**], and $[Et_4N]_4$[**4a**] are listed in Supporting Information, Table S2.

Electrochemical Measurements. The CV measurements were performed at room temperature under a nitrogen atmosphere and recorded using a BAS-100W electrochemical potentiostat. A glassy carbon working electrode, a platinum wire auxiliary electrode, and a nonaqueous Ag/Ag^+ electrode were used in a three-electrode configuration. Tetra-*n*-butylammonium perchlorate (TBAP) was

(29) Blessing, R. H. *Acta Crystallogr., Sect. A* **1995**, *51*, 33.
(30) North, A. C. T.; Philips, D. C.; Mathews, F. S. *Acta Crystallogr.* **1968**, *A24*, 351.
(31) Sheldrick, G. M. *SHELXL97, version 97−2*; University of Göttingen: Göttingen, Germany, 1997.

Table 5. Crystallographic Data for $[Et_4N]_2[SeFe_3(CO)_9CuCl]$ ($[Et_4N]_2$[**1a**]), $[Et_4N]_2[SeFe_3(CO)_9CuBr]$ ($[Et_4N]_2$[**1b**]), $[Et_4N]_2[SeFe_3(CO)_9CuI]$ ($[Et_4N]_2$[**1c**]), $[Et_4N]_2[SeFe_3(CO)_9Cu_2Cl_2]$ ($[Et_4N]_2$[**2a**]), $[Et_4N]_2[SeFe_3(CO)_9Cu_2Br_2]$ ($[Et_4N]_2$[**2b**]), $[Et_4N]_2[\{SeFe_3(CO)_9\}_2Cu_4Cl_2]$ ($[Et_4N]_2$[**3a**]), $[PPh_4]_2[\{SeFe_3(CO)_9\}_2Cu_4Br_2]$ ($[PPh_4]_2$[**3b**]), and $[Et_4N]_4[\{SeFe_3(CO)_9(CuCl)_2\}_2]$ ($[Et_4N]_4$[**4a**])

	$[Et_4N]_2$[**1a**]	$[Et_4N]_2$[**1b**]	$[Et_4N]_2$[**1c**]
empirical formula	$C_{25}H_{40}ClCuFe_3N_2O_9Se$	$C_{25}H_{40}BrCuFe_3N_2O_9Se$	$C_{25}H_{40}ICuFe_3N_2O_9Se$
fw	858.09	902.55	949.54
cryst syst	monoclinic	monoclinic	monoclinic
space group	$P2_1/a$	$P2_1/a$	$P2_1/a$
cryst dimensions (mm)	0.65 × 0.45 × 0.40	0.35 × 0.30 × 0.18	0.45 × 0.40 × 0.35
a (Å)	18.9503(3)	18.7266(2)	19.34(1)
b (Å)	9.9521(2)	10.0586(1)	10.006(2)
c (Å)	19.7374(5)	19.9630(3)	20.407(7)
α (deg)			
β (deg)	113.002(1)	113.16(4)	114.28(4)
γ (deg)			
V (Å^3)	3426.4(1)	3457.44(7)	3599(2)
Z	4	4	4
D_{calcd} (g cm^{-3})	1.663	1.734	1.752
μ ($Mo_{K\alpha}$) (mm^{-1})	3.045	4.096	3.682
diffractometer	Nonius (Kappa CCD)	Nonius (Kappa CCD)	Nonius (CAD4)
radiation (λ) (Å)	0.71073	0.71073	0.71073
temp (K)	200	200	298
θ range for data collecn (deg)	2.16−25.40	2.18−25.04	2.11−24.92
T_{min}/T_{max}	0.19/0.30	0.28/0.37	0.19/0.27
no. of indep reflns	4697 ($I > 2\ \sigma(I)$)	5061 ($I > 2\ \sigma(I)$)	3735 ($I > 2\ \sigma(I)$)
no. of parameters	364	379	379
R1[b]/wR2[b] ($I > 2\ \sigma(I)$)	0.0752/0.2034	0.0362/0.0979	0.0485/0.1285
R1[b]/wR2[b] (all data)	0.0994/0.2326	0.0550/0.1275	0.1020/0.1497

	$[Et_4N]_2$[**2a**]	$[Et_4N]_2$[**2b**]	$[Et_4N]_2$[**3a**]
empirical formula	$C_{17}H_{20}Cl_2Cu_2Fe_3NO_9Se$[a]	$C_{25}H_{40}Br_2Cu_2Fe_3N_2O_9Se$	$C_{34}H_{40}Cl_2Cu_4Fe_6N_2O_{18}Se_2$
fw	826.83	1046.00	1582.76
cryst syst	monoclinic	monoclinic	orthorhombic
space group	$P2_1/n$	$P2_1/n$	$Pcan$
cryst dimensions (mm)	0.28 × 0.22 × 0.06	0.35 × 0.18 × 0.14	0.65 × 0.45 × 0.40
a (Å)	24.2470(3)	24.562(4)	12.168(4)
b (Å)	10.7879(2)	10.926(4)	17.759(8)
c (Å)	28.1333(5)	28.563(4)	24.18(1)
α (deg)			
β (deg)	99.309(1)	99.60(1)	
γ (deg)			
V (Å^3)	7262.0(2)	7558(3)	5225(4)
Z	8	8	4
D_{calcd} (g cm^{-3})	1.513	1.839	2.012
μ ($Mo_{K\alpha}$) (mm^{-1})	3.505	5.354	4.767
diffractometer	Nonius (Kappa CCD)	Nonius (CAD4)	Nonius (CAD4)
radiation (λ) (Å)	0.71073	0.71073	0.71073
temp (K)	200	298	298
θ range for data collecn (deg)	2.06−25.37	1.68−23.92	1.68−24.94
T_{min}/T_{max}	0.42/0.63	0.34/0.47	0.07/0.15
no. of indep reflns	8363 ($I > 2\ \sigma(I)$)	4142 ($I > 2\ \sigma(I)$)	3461 ($I > 2\ \sigma(I)$)
no. of parameters	619	793	307
R1[b]/wR2[b] ($I > 2\ \sigma(I)$)	0.0823/0.2337	0.0503/0.0994	0.0291/0.0688
R1[b]/wR2[b] (all data)	0.1192/0.2589	0.2392/0.1481	0.0517/0.0750

	$[PPh_4]_2$[**3b**]	$[Et_4N]_4$[**4a**]
empirical formula	$C_{66}H_{40}Br_2Cu_4Fe_6P_2O_{18}Se_2$	$C_{42}H_{60}Cl_4Cu_4Fe_6N_3O_{18}Se_2$[a]
fw	2089.92	1783.91
cryst syst	triclinic	triclinic
space group	$P\bar{1}$	$P\bar{1}$
cryst dimensions (mm)	0.23 × 0.16 × 0.14	0.32 × 0.12 × 0.07
a (Å)	11.4539(2)	13.1869(2)
b (Å)	12.0389(2)	16.9800(3)
c (Å)	14.2813(3)	18.2612(3)
α (deg)	106.474(1)	70.158(1)
β (deg)	90.812(1)	76.507(1)
γ (deg)	105.142(1)	68.605(1)
V (Å^3)	1814.57(6)	3553.0(1)
Z	1	2
D_{calcd} (g cm^{-3})	1.913	1.667
μ ($Mo_{K\alpha}$) (mm^{-1})	4.523	3.589
diffractometer	Nonius (Kappa CCD)	Nonius (Kappa CCD)
radiation (λ) (Å)	0.71073	0.71073
temp (K)	298	200
θ range for data collecn (deg)	2.22−25.06	2.17−25.09
T_{min}/T_{max}	0.40/0.48	0.46/0.64
no. of indep reflns	4984 ($I > 2\ \sigma(I)$)	8794 ($I > 2\ \sigma(I)$)
no. of parameters	452	711
R1[b]/wR2[b] ($I > 2\ \sigma(I)$)	0.0345/0.0822	0.0557/0.1511
R1[b]/wR2[b] (all data)	0.0543/0.0972	0.0810/0.1634

[a] One cationic molecule, Et_4N^+, is excluded in the formula, formula weight, calculated density, μ, F(000), and R1/wR2 according to the Platon Squeeze procedure. [b] The functions minimized during least-squares cycles were $R1 = \sum||F_o| - |F_c||/\sum|F_o|$ and $wR2 = [\sum[w(F_o^2 - F_c^2)^2]/\sum[w(F_o^2)^2]]^{1/2}$.

used as the supporting electrolyte, and the solute concentration was $\sim 10^{-4}$ M. The redox potentials were calibrated with a ferrocenium/ferrocene (Fc^+/Fc) couple in the working solution and referenced to SCE.

Computational Details. Calculations reported in this study were performed via DFT[20,21] using the Gaussian 03[32] series of packages. The geometries of complexes $[SeFe_3(CO)_9]^{2-}$, **1a**−**1c**, **2a**, **2b**, **3a**, **3b**, and **4a** were taken from single-crystal XRD data. All geometries were calculated at B3LYP/LanL2DZ level. In addition, the proposed intermediates **2a′** and **4a′** were fully optimized with the same level of theory. Wiberg bond indices[23] and natural charges[24] were evaluated with Weinhold's NBO method.[33] Graphical representations of the molecular orbitals were obtained using CS Chem3D 5.0.

Acknowledgment. This work was supported by the National Science Council of Taiwan (NSC Grant 95-2113-M-003-009-MY3 to M.S.). We are also grateful to the National Center for High-Performance Computing, where the Gaussian package and computer time were provided. Our gratitude also goes to the Academic Paper Editing Clinic, NTNU.

Supporting Information Available: X-ray crystallographic files in CIF format for $[Et_4N]_2$[**1a**], $[Et_4N]_2$[**1b**], $[Et_4N]_2$[**1c**], $[Et_4N]_2$[**2a**], $[Et_4N]_2$[**2b**], $[Et_4N]_2$[**3a**], $[PPh_4]_2$[**3b**], and $[Et_4N]_4$[**4a**], computational details for complexes $[SeFe_3(CO)_9]^{2-}$, **1a**−**1c**, **2a**, **2b**, **3a**, **3b**, and **4a** and the optimized geometries of **2a′** and **4a′**, and electrochemical and PXRD data. This material is available free of charge via the Internet at http://pubs.acs.org.

IC8012552

(32) Frisch, M. J.; Trucks, G. W.; Schlegel, H. B.; Scuseria, G. E.; Robb, M. A.; Cheeseman, J. R. ; Montgomery J.A., Jr.; Vreven, T.; Kudin, K. N.; Burant, J.C.; Millam, J. M.; Iyengar, S. S.; Tomasi, J.; Barone, V.; Mennucci, B.; Cossi, M.; Scalmani, G.; Rega, N.; Petersson, G. A.; Nakatsuji, H.; Hada, M.; Ehara, M.; Toyota, K.; Fukuda, R.; Hasegawa, J.; Ishida, M.; Nakajima, T.; Honda, Y.; Kitao, O.; Nakai, H.; Klene, M.; Li, X.; Knox, J. E.; Hratchian, H. P.; Cross, J. B.; Bakken, V.; Adamo, C.; Jaramillo, J.; Gomperts, R.; Stratmann, R. E.; Yazyev, O.; Austin, A. J.; Cammi, R.; Pomelli, C.; Ochterski, J. W.; Ayala, P. Y.; Morokuma, K.; Voth, G. A.; Salvador, P.; Dannenberg, J. J.; Zakrzewski, V. G.; Dapprich, S.; Daniels, A. D.; Strain, M. C.; Farkas, O.; Malick, D. K.; Rabuck, A. D.; Raghavachari, K.; Foresman, J. B.; Ortiz, J. V.; Cui, Q.; Baboul, A. G.; Clifford, S.; Cioslowski, J.; Stefanov, B. B.; Liu, G.; Liashenko, A.; Piskorz, P.; Komaromi, I.; Martin, R. L.; Fox, D. J.; Keith, T.; Al.Laham, M. A.; Peng, C. Y.; Nanayakkara, A.; Challacombe, M.; Gill, P. M. W.; Johnson, B.; Chen, W.; Wong, M. W.; Gonzalez, C.; Pople, J. A. *Gaussian 03*, revision B.04; Gaussian, Inc.: Wallingford CT, 2004.

(33) Reed, A. E.; Curtiss, L. A.; Weinhold, F. *Chem. Rev.* **1988**, *88*, 899.